Quantum interference in an organic solid

Niklas Christensson

Master Thesis
Carried out at Montana State University,
Bozeman, MT, USA

LUND
UNIVERSITY

Abstract

Interference of probability amplitudes constitutes one of the fundamentals of quantum mechanics leading to some of the most intriguing phenomena in quantum optics such as electromagnetically induced transparency. Here we demonstrate quantum interference between one- and three-photon transition amplitudes in an organic solid at room temperature. To produce the interference, we apply a near-IR beam of frequency ω, intersecting at a small angle with a harmonically derived UV beam of frequency 3ω, on a thin polymer film containing fluorescing organic molecules. The sample molecules are specially designed to have a high efficiency of three-photon absorption at near IR wavelengths. The high visibility spatial interference pattern, formed in the intensity of the fluorescence, is readily detected with a CCD camera, and can even be seen with the naked eye.

The high visibility of the fringe pattern arises from the fact that the probability amplitudes of one- and three-photon absorption can be made comparable, which is possible due to the high efficiency of three-photon absorption in the special organic molecule doped into the polymer film. This molecule, together with two series of different organic molecules with related structure, was characterized by one- and three-photon spectroscopy, showing that it has one of the largest three-photon cross sections measured to this date, due to a unique two-dimensional π-conjugated electron structure. The spectroscopic studies also show that the three-photon excitation spectrum does not always follow the one-photon spectrum as predicted by perturbation theory. A new and simple model is introduced to explain the results.

Our experiment serves as an extension of Young's double slit experiment to the case of quantum mechanical interference between two different wavelengths.

Keywords: *Quantum Interference, Optical nonlinearities in organic materials, Three-photon spectroscopy, π-conjugated molecules.*

Acknowledgements

Table of contents

1. Introduction

Interference is a fundamental physical property that explains a number of everyday observations and is a cornerstone of modern quantum mechanics. Young's double slit experiment is perhaps the most important experiment of the 19: th century, revealing the dual nature of light. Understanding of the Young experiment lead to a number of new experiments and a widened knowledge about the surrounding world. Optical interference is only a special case of interference involving light. Any system that can transfer from one state to another in more than one way will show interference. Here we make a distinction between optical interference and quantum interference. In optical interference there are two different optical pathways connecting the ground- and excited state with one transition. Experiments like Young's double slit belongs in this category. In quantum interference, the same initial and final states are connected by two different quantum pathways. Manykin predicted as early as 1967 [1], that interference can occur between two alternative excitation pathways, in which an atom is brought to an excited state by simultaneously absorbing either one (3ω) or three (ω) photons. We would normally expect that a fundamental (IR) and its third harmonic (UV) would lead to transitions between different initial- and final-states. Since most known material are notoriously weak multiphoton absorbers, this is generally the case. However, if one uses a system (molecule) with a high three-photon cross section in combination with an intensive fundamental beam, then $3\omega+\omega$ interference could in principle be observed.

The first experiments on this kind of interference were made in gas phase on atomic vapors under high intensity conditions. The experiments showed that the rate of absorption (probed by ionization) varied periodically as the relative phase of the two laser fields was varied. A number of experiments have demonstrated this effect in atomic vapors and in small molecules in gas phase [2-3]. These first experiments were dealing with bound-bound transitions. It was later realized that bound-continuum transitions could lead to selective chemistry. The excitation scheme can lead to control of the dissociation/ionization of small molecules like HI (in gas phase). In the case of HI it has been shown that either ionization or dissociation can be enhanced by varying the relative phase of the two fields [4]. This opened up the possibility of coherent control of chemical reactions [5-7] [I][1]. Although this field has seen an enormous growth over the past 15 years there has been little progress for this control scenario.

---

[1] Arabic numbers refers to references, see p. 77. Roman numbers refers to notes on p. 62

The goal of this work is to observe $3\omega+\omega$ interference in an organic solid at room temperature. Very little attention has been devoted to $3\omega+\omega$ interference in condensed phase, not only due to the problems with weak three-photon absorbers but also due to the problems associated with dispersion. Since the phase of the 3ω and ω fields will change at a different rate in a dispersive medium, the initial phase relation will be lost for a thicker sample. The observed signal is generally a sum of contributions from the entire sample and regions that are "out" of phase will cancel regions that are "in" phase. Recently Fraser et al [8] studied both the $3\omega+\omega$ and $2\omega+\omega$ scenario in bulk GaAs where they were able to control the free carrier density by varying the relative phase of the two fields used for excitation. They avoided the dispersion problem by growing sub-micrometer films. GaAs is a weak three-photon absorber and this fact limited their control of the carrier density.

From this brief discussion it stands clear that a number of experimental difficulties must be overcome in order to succeed. First of all it is necessary to use a laser system with high peak power, and a fs system is the natural choice. The two beams used for excitation must be mutually coherent and one needs to derive the third harmonic, from the fundamental, by a coherent process. It is important that the pulses have approximately the same duration (and shape) since the visibility of the interference pattern will depend on the temporal overlap between the pulses. The second difficulty lies in finding a sample that is an efficient three-photon absorber. These two requirements have up until now been the largest obstacles associated with observing quantum interference between ω and 3ω transitions. The third difficulty is preparing a sample that is thin enough so that the dispersion does not destroy the visibility of the interference fringes.

This thesis is prepared as follows: Section 2 gives an introduction to multiphoton absorption in the frame work of the semi-classical approximation. This section also includes a discussion about third harmonic generation and the properties of conjugated organic molecules. The laser system used for the experiment is described in section 3. Section 4 is devoted to the search for a suitable molecular system and includes spectroscopic studies of two series of organic molecules. Section 5 deals with the results of the quantum interference experiment. This section is concluded by a discussion about other observations of quantum interference (resonant third harmonic generation) and the analogy to Young's double slit experiment.

Description of experimental details, such as measurement of the pulse duration of the fundamental and the third harmonic pulses, are important but has, due to their technical nature, been collected in an Appendix.

2. Theory

2.1 Introduction to Multi-photon Absorption

Perhaps the simplest way to consider multiphoton absorption is by writing down a simple equation for the change of the intensity of an electromagnetic field as a function of propagation distance:

$$\frac{dI}{dz} = -\alpha I - \beta I^2 - \gamma I^3 \dots \quad (2.1.1)$$

, where α, β, γ are the one-, two- and three-photon absorption coefficients. The higher order coefficients are always small and can be neglected unless the intensity of the wave is high. In the limit of low intensity one recovers Beer-Lambert law and the intensity decays exponentially as a function of propagation distance. Since all coefficients are wavelength dependent, there will be a wavelength region where α and β can be neglected, (usually in the NIR range), and the only way a molecule can transfer to the excited state is by three-photon absorption. The solution of equation 2.1.1 in this case will be:

$$I(z) = \frac{I_0}{\sqrt{1 + 2\gamma z I_0^2}} \quad (2.1.2)$$

where I_0 is the intensity at the entrance of the medium. Because γ is typically very small, the denominator will, for most cases be close to unity and the beam will experience little attenuation as it passes through the medium. This can be verified experimentally when observing three-photon fluorescence from a thick sample. The three-photon excited fluorescence is emitted from the entire sample length in striking contrast to when the sample is excited with the third harmonic (i.e linear excitation).

Equation 2.2.1 does not provide insight to the microscopic phenomenon governing the three-photon absorption process. The transition rates for three-photon absorption can be calculated from perturbation theory. Such derivations can be found in [9-11] and we will only quote the necessary results.

If, at time t=0, an atom or molecule in it's ground state |g>, interacts with a monochromatic beam of frequency ω, then the probability amplitude of finding the system at time t in the excited state, |e>, can be written, for one and three-photon absorption respectively, as:

$$a_{eg}^{(1)} = \frac{\mu_{eg} \cdot \varepsilon \cdot E}{2\hbar} \left(\frac{e^{i(\omega_{eg} - \omega_3)t} - 1}{\omega_{eg} - \omega_3} \right) \quad (2.1.3)$$

$$a_{eg}^{(3)} = \frac{1}{8\hbar^3} \sum_{n,m} \frac{(\mu_{ng} \cdot \varepsilon)(\mu_{mn} \cdot \varepsilon)(\mu_{me} \cdot \varepsilon)E^3}{(\omega_{mg} - \omega)(\omega_{ng} - 2\omega)} \left(\frac{e^{i(\omega_{eg} - 3\omega)t} - 1}{\omega_{eg} - 3\omega} \right) \quad (2.1.4)$$

where ϵ is a polarization vector and $\omega_3 = 3\omega$. Equation 2.1.4 assumes a single source for excitation and the rotating wave approximation has been used to simplify the calculations. The two excitation paths are shown in figure 2.1.
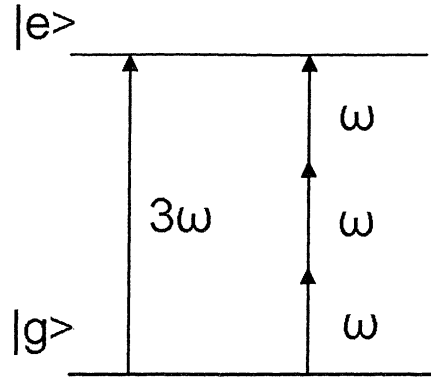
Figure 2.1.1 Different excitation mechanisms. State n and m are virtual for direct multiphoton absorption and are omitted in the picture which means that there are no real intermediate resonances.

The double sum in and (2.1.4) includes all states of the molecule. We can also see that the transition amplitudes can be enhanced if there is an intermediate level between the ground state and the first excited state. The influence of intermediate resonances is well illustrated in anthracene-porphyrin-antracene triad [12] where the three-photon transition is doubly resonant. Calculations show that addition of the two anthracene molecules leads to an increase in the three-photon cross section by two orders of magnitude compared to the sum of the individual cross sections. The three-photon cross section has not yet been measured and it will be difficult since the two- and three-photon absorption bands overlap. The calculated value, $\sigma_3 = 10^{-77} \, \text{cm}^6\text{s}^2$, is one order of magnitude larger than any measured cross section.

Since it is the probability of excitation rather than the transition amplitude that will determine the response of the system, we need to consider the square modulus of the transition amplitude. For three-photon absorption we find:

$$P(t) = \left| a_{eg}^3 \right|^2 = \left(\frac{1}{\hbar^3} \sum_{n,m} \frac{(\mu_{em} \cdot \varepsilon_1)(\mu_{nm} \cdot \varepsilon_2)(\mu_{gn} \cdot \varepsilon_3)E^3}{(\omega_{mg} - \omega)(\omega_{ng} - 2\omega)} \right)^2 \left| \left(\frac{e^{i(\omega_{mg} - 3\omega)t} - 1}{\omega_{eg} - 3\omega} \right) \right|^2 \quad (2.1.5)$$

The time dependent part of (2.1.5) will become sharply peaked in the limit $t \rightarrow \infty$ and its limiting value is [9-10] [II]:

8

$$\lim_{t \to \infty} \left| \left(\frac{e^{i(\omega_{eg} - 3\omega)t} - 1}{\omega_{eg} - 3\omega} \right) \right|^2 = 2\pi t \delta(\omega_{eg} - 3\omega) \ (2.1.6)$$

The transition probability is infinite at resonance and this is clearly not physical. For non interacting molecules the peak value of the cross section is limited by the radiative lifetime of the excited state, |e>. In organic solids, additional line broadening mechanisms like de-phasing and non-radiative decay further reduces the peak value.

If the upper level to consist of a continuous distribution of states, then the delta function should be replaced with a suitable normalized line shape function $g(\omega_{eg} - 3\omega)$. A Gaussian function is well suited for describing the line shape of electronic transitions amorphous organic solid material.

To calculate the transition probability created by an arbitrary pulse shape, $E(t)e^{-i\omega t}$ one must calculate the integral of the rate, $P(t)/t$, over all times. We thus have:

$$P_3(t) = \left(\frac{1}{\hbar^3} \sum_{n,e} \frac{(\mu_{eg} \cdot \varepsilon_1)(\mu_{ne} \cdot \varepsilon_2)(\mu_{mn} \cdot \varepsilon_3)}{(\omega_{eg} - \omega)(\omega_{ng} - 2\omega)} \right)^2 2\pi g(\omega_{eg} - 3\omega) \int_t |E(t)|^6 dt \ (2.1.8)$$

Equation (2.1.8) clearly states that the probability of transition depends in a non-linear fashion on the applied field and that it is the peak power rather than the average power that is important.

In the literature it is more common to use the photon flux rather than the electric field amplitude which leads to the introduction of a molecular cross section, σ_3. The photon flux and electric field are related through:

$$E = \sqrt{\frac{\hbar\omega}{2n}} \sqrt{\frac{\mu_0}{\varepsilon_0}} F \ (2.1.9)$$

The probability can now be written as:

$$P_3(t) = \left(\frac{1}{\hbar^3} \sum_{n,e} \frac{(\mu_{eg} \cdot \varepsilon_1)(\mu_{ne} \cdot \varepsilon_2)(\mu_{mn} \cdot \varepsilon_3)}{(\omega_{eg} - \omega)(\omega_{ng} - 2\omega)} \right)^2 2\pi \left(\frac{\hbar\omega}{2n} \sqrt{\frac{\mu_0}{\varepsilon_0}} \right)^3 \int_t F(t)^3 dt \cdot g(\omega_{eg} - 3\omega) \ (2.1.10)$$

$$= \sigma_3 \int F^3(t) dt \cdot g(\omega_{eg} - 3\omega)$$

Now, all the molecular properties are contained within the cross section, σ_3, and it is this quantity that is measured experimentally [III]. The unit for this cross section is $cm^6 s^2$, and typical measured values rages from $\sigma_3 \approx 10^{-82}$ cm^{6}s^2 for small molecules like benzene to $\sigma_3 \approx 10^{-78}$ cm^{6}s^2 for larger conjugated molecules.

If the molecules emit fluorescence, then we can write the number of emitted fluorescence photons due to three-photon excitation as:

$$F^{3PA} = \frac{1}{3}\eta_F \sigma_3 ANz \int F_f^3 dt = \frac{1}{3}\eta_F \sigma_3 ANz F_f^3 \tau \quad (2.1.11)$$

where η_F is the quantum yield of fluorescence, A is the beam cross section, F is the photon flux, τ is the pulse duration and N and z is the number concentration and the propagation distance, respectively. It is implicitly assumed that the nonlinear absorption is weak and that the pulse is of rectangular shape. The 1/3 factor is a convention arising from the fact that three photons are needed to excite one molecule.

Most samples are isotropic and we must consider averaging over the spatial orientation of the molecules dipole moment vectors with respect to the direction of the polarization vector of the laser field. Performing isotropic averaging for arbitrary relative directions of the dipole moments of different transitions is a fairly complicated matter. Here we assume that, in the molecular frame, all dipole moments are pointing in the same direction and that there are no (real) intermediate resonances. This greatly simplified two level model has proven to describe three-photon absorption well for similar molecular systems. The sum over all states in equation 2.1.8 thus reduces to a sum over two states and one finds that the sum in equation 2.1.8 can be written as:

$$\left(\frac{1}{\hbar^3} \sum_{n,e} \frac{(\mu_{eg} \cdot \varepsilon)(\mu_{ne} \cdot \varepsilon)(\mu_{mn} \cdot \varepsilon)}{(\omega_{eg} - \omega)(\omega_{ng} - 2\omega)} \right)^2 = \left(\frac{1}{\hbar^3} \frac{2d^2(\mu_{mg} \cdot \varepsilon) - (\varepsilon \cdot \mu_{mg})^3}{4\omega_{mg}^2} \right)^2 \quad (2.1.12)$$

Where we have introduced d as the difference in permanent dipole moment between the ground state and the (first) excited state (multiplied with the polarization vector). The molecules used in this work are almost non-polar and therefore have no permanent dipole moment and d=0 is thus a good assumption. The word "dipole moment" will in the rest of this paper refer to *transition* dipole moments, if nothing else is explicitly stated.

The averaging procedure is now simple and one finds:

$$\left(\mu_{mg} \cdot \varepsilon \right)^6 = \left| \mu_{mg} \right|^6 \int \cos^6(\alpha) d\alpha = \frac{1}{7} \left| \mu_{mg} \right|^6 \quad (2.1.13)$$

We see that the three-photon cross section is proportional to the sixth power of the dipole moment. In comparison, the linear cross section is proportional to the square of the (same) dipole moment. Therefore we can write, in first approximation:

$$\sigma_3 \propto \frac{f_{eg}^3}{\omega_{eg}^4} g\left(\omega_{eg} - 3\omega\right), (2.1.14)$$

where f_{eg} and ω_{eg} are the linear oscillator strength and transition frequency respectively. We can conclude that a strong linear absorber is also a strong three-photon absorber. The difference between strong and weak absorbers is clearer in the three-photon absorption process due to the higher power dependence on the dipole moment.

2.2 Simultaneous One- and Three-photon Absorption

Even if one has a molecule with a large σ_3 the probability of three-photon absorption is still rather low, and it might seem more favorable to look for interference between two photon absorption and linear absorption, i.e. $2\omega+\omega$ interference rather than $3\omega+\omega$. However, in order for one- and two-photon absorption to take place between the same initial and final state one needs a non symmetric molecule to relax the parity selection rule [IV]. The situation becomes even worse when rotational averaging is taken into account. The interference term will average to zero in the first approximation [13-14]. One thus needs a sample that is non symmetric on both the micro and macro scale. This can be achieved by using a non symmetric molecule and ordering the sample with electrical- or optical-poling [15-17]. The poling techniques are not very efficient and it seems like the chance of observing interference is greater for the $3\omega+\omega$ scenario even if this scenario has higher requirements on the incident intensity.

We now turn to the main problem of this text, quantum interference between one- and three-photon transition amplitudes. We want to calculate the probability for this kind of event. There is clearly more then one way that the molecule can transfer to the excited state and the total probability of excitation is the square modulus of the sum of the transition amplitudes. We therefore start out with two linearly polarized fields of frequency ω and 3ω. The propagation distance in the quantum interference experiment will be very short and we can neglect the fact that the two pulses travel with different group velocity. We also make use of the slowly varying amplitude approximation and neglect the rapid oscillations and work with envelop functions.

$$E_1 = \frac{1}{2}\varepsilon \cdot E_1(t-\tau)\left(e^{-i\omega_1 t + k_1 z + \varphi_1} + cc.\right)$$

$$E_3 = \frac{1}{2}\varepsilon \cdot E_3(t)\left(e^{-i\omega_3 t + k_3 z + \varphi_3} + cc.\right)$$

$$(2.2.1)$$

where E_1 and E_3 are the (real) envelope of the fundamental (IR) and the third harmonic (UV) pulse, respectively. As usual, ω and k refer to the angular frequency and the wave vector of each pulse and ϵ is a polarization vector. Taking the transition amplitudes from section 2.1 we can write the joint probability for a transition from state g to e:

$$P = \left|a_{eg}^{(1)}(t) + a_{eg}^{(3)}(t)\right|^2 \quad (2.2.2)$$

Substituting equation (7.1.1) into equation (7.1.2) gives after rather lengthy calculations and simplifications:

$$P = \int \left(\begin{matrix} \left(\frac{\mu_{eg}\cdot\varepsilon}{2\hbar}\right)^2 |E_3(t)|^2 + \left(\frac{1}{8\hbar^3}\sum_{mn}\frac{(\mu_{em}\cdot\varepsilon)(\mu_{mn}\cdot\varepsilon)(\mu_{mg}\cdot\varepsilon)}{(\omega_{ne}-\omega)(\omega_{me}-2\omega)}\right)^2 \left|E_1^3(t-\tau)\right|^2 + \\ 2\frac{\mu_{eg}\cdot\varepsilon}{4\hbar}\cdot\frac{1}{\hbar^3}\sum_{m,n}\frac{(\mu_{em}\cdot\varepsilon)(\mu_{mn}\cdot\varepsilon)(\mu_{mg}\cdot\varepsilon)}{(\omega_{ne}-\omega)(\omega_{me}-2\omega)}\cdot\left|E_3(t)E_1^3(t-\tau)\right|\cdot\cos((k_3-3k_1)r+\Delta\varphi) \end{matrix} \right) \cdot \left(\frac{e^{i(\omega eg-3\omega_1)t}-1}{\omega_{eg}-\omega}\right)^2 dt$$

$$(2.2.3)$$

where $(k_3-3k_1)r$ can be interpreted as a relative phase between the fields. It is clear that the expression contains three terms. The first and second term corresponds to linear- and three-photon absorption, respectively. The third term is an interference term and we can clearly see that this term is dependent on the relative phase of the two fields. It should be noted that the amplitude of the interference term depends on the temporal overlap of the fundamental and the third harmonic.

We find that all three terms can be described by a common line shape function that can be introduced in a similar fashion to the case of three-photon absorption. Since this kind of operation does not add anything to our discussion, this part will be omitted in the following calculations.

Assuming that all dipole moments are parallel to the laser light, thus reducing the isotropic averaging to calculating the average of cosine functions of different powers. One find the coefficients $1/3$, $1/7$, $1/5$ for the three terms in equation 2.2.3 [13]. Rewriting the probability using the cross sections gives (The rotational averaging is implicitly included in the experimentally measured cross sections and the factor $\sqrt{21}$ originates from writing the interference terms using the cross sections):

$$P = \int \left[\sigma_1 F_3(t) + \sigma_3 F_1^3(t-\tau) + \frac{2\sqrt{21}}{5}\sqrt{\sigma_1\sigma_3}F_3^{1/2}(t)F_1^{3/2}(t-\tau)\cos\big((k_3 - 3k_1)r\big) \right] dt$$

(2.2.4)

The expression (2.2.4) can, in the limit of low absorption, be generalized by taking into account the spatial variations of the field and letting the integral go over both (all) space and time (see section 5).

We note that the same result as equation 2.2.4 is obtained by a more elaborate calculation using density matrix equations in the rate approximation [18].

2.3 Third Harmonic Generation

Third harmonic generation is a $\chi^{(3)}$ process which it is not restricted to materials without a center of symmetry and is thus present in all optical material such as glass, polymers etc. Even if the process is not phase matched, it can still be relatively efficient under the conditions of excitation with high intensity femtosecond pulses, up to one percent. If three times the frequency of the input beam is resonant with a transition in the material, then the third harmonic generation can be followed by one photon absorption. It is very difficult to separate this process from direct three-photon absorption since the power dependence is the same for both processes, i.e. $P \propto I^3$. No simple measurement can determine which of the two processes that dominates. Also, because the sample is often strongly absorbing at the third harmonic frequency, the lack of third harmonic in transmission does not always guarantee that this process can be neglected.

To gain some more insight, we consider the process of resonant third harmonic generation using the amplitude equations for a CW field. In order to simplify the calculations, we assume that the slowly varying amplitude approximation is valid and that the field is monochromatic. We further assume that the incident beam experiences little attenuation and can be assumed constant (undepleted pump approximation). The coupled amplitude equations [9] thus reduce to one simple equation. Since the process is resonant, linear absorption must be included for the third harmonic. The equation for the change in the field is:

$$\frac{dA_3}{dz} = i\frac{\mu_0\varepsilon_0\omega_3^2}{2k_3}\chi^{(3)}A_1^3 \cdot e^{i(3k_1-k_3)z} - aA_3 \quad (2.3.1)$$

As usual, ω and k is the frequency and wave vector of the fields. $\chi^{(3)}$ is the third order susceptibility of the medium and $\alpha = 2a$ is the absorption coefficient.

Solving equation 7.5.1 is straight forward and one finds:

$$I_{3\omega} = \left| A_3 A_3^* \right|^2 = \frac{1}{\alpha^2 + \Delta k^2} \frac{2\pi n_3 \omega_3^4}{k_3^2 c^3} \left| \chi^{(3)} \right|^2 \left| A_1 \right|^6 \left(e^{-2\alpha z} - 2e^{-\alpha z} \cos(\Delta kz) + 1 \right) (2.3.2)$$

where $\Delta k = 3k_1 - k_3$ is the wave vector mismatch between fundamental and third harmonic.

For the limiting case of low absorption the intensity (2.3.2) is an oscillating function due to the wave vector mismatch. In the limit of large absorption, I_3 saturates quickly and the transmitted third harmonic is independent of propagation length.

It is very instructive to expand the susceptibility as:

$$\chi^{(3)} = \langle \gamma \rangle N \; (2.3.3)$$

where $\langle \gamma \rangle$ is the averaged third order polarizability. We can substitute this expression into 2.3.2 and we find that the amount of third harmonic is proportional to the number concentration squared. This should be compared to the three-photon absorption process that has a linear dependence on the concentration. This difference in concentration dependence can be used to distinguish between the two processes discussed above. This is, however, not as straight forward as it might seem. Possible ways for distinguish between the two processes will be discussed in section A1.

2.4 Nonlinear Optics of Conjugated Molecules

Almost all known materials are weak multiphoton absorbers. This can be understood from the expression (2.1.14) for the cross section in the previous section. The dipole moment enters the expression in the sixth power and it should be clear that a large dipole moment is necessary in order to have a good multiphoton absorber. It is also clear that good linear absorbers have larger dipole moment and it is natural to look amongst material with strong linear absorption when searching for a multi-photon absorbing material. Organic molecules have dipole moments that often are orders of magnitude larger than the dipole moment of a typical atomic transition. The perhaps best known molecules are the (laser) dyes which all have a very strong absorption and thus large dipole moments. Most of these dyes are organic compounds with extended π-conjugation which gives them special optical properties [22]. The concept of conjugated systems arises from the two types of bonds associated with chemical bonding, the π- and σ-bonds. σ-bonds are generally stronger then π- bonds and the corresponding bond energy is well above the visible region. The π-bonds also differ from the σ-bonds in that they are de-localized, i.e. their spatial confinement is not as limited as the σ-bonds. This has a

profound effect on their behavior when exposed to an external electromagnetic field. Since the π-electrons are more loosely bond they are also more susceptible to perturbations making them well suited for nonlinear optics. The importance of de-localization on the dipole moment is readily understood from the expression for the transition dipole moment,

$\mu_{eg} = e \int \Psi_e \cdot r \cdot \Psi_g dr$, which clearly has a larger value for a more de-localized wave function due to the weighting factor r.

The simplest conjugated system is a chain of carbon atoms with alternating single and double bonds (a polymer). While the σ-bonds are confined to the space between the carbon atoms, the π-electrons are free to move from atom to atom such that it is not possible to assign a specific electron to a certain atom. For an ideal polymer this de-localization can extend over the entire molecule. It can be shown that the nonlinear response of the polymer grows very rapidly as the length of the π-conjugation increases (5:th power for third order susceptibility) [9]. What in reality limits the de-localization is the "flatness" of the polymer. If the chain twists in space, then the π-electrons cannot de-localize over the entire molecule and the conjugation is broken. This loss of conjugation limits the collective response of these electrons and this has a profound effect on the nonlinear properties. We shall not talk too much about the strategy for designing molecules with enhanced nonlinear optical response but we conclude that in order to obtain high nonliearities it is important that the molecule is fully conjugated. The key issue in designing large molecules for non-linear optics is to stabilize the molecule in such a way that it preserves its planar structure. This can be done in different ways as illustrated by the chemical formulas in appendix A (triflurino- groups or triple bonds).

The nonlinear optical properties of linear polymers are well known as they have been studied extensively over the years [20]. A more interesting class is molecules with dendric (branching) structure. The dendric molecules are interesting for a number of reasons. The branching structure facilitates the chemical variation of different attachment groups and this can lead to the combination of different types of properties. A very interesting example is the addition of groups that are efficient in producing singlet oxygen to an efficient multi-photon absorber thus opening for multi-photon photodynamic therapy [11]. The dendric molecules also offer a higher packing density than linear molecules. Another interesting feature is the nonlinear enhancement observed in dendrimers [21]. It has been verified experimentally that the nonlinear absorption cross section grows faster than the sum of the individual subunits.

This type of nonlinear enhancement requires that the π-conjugation extends to adjacent branches of the dendrimer.

The molecules used in this paper are all nitrogen branched. The nitrogen atom in these molecules does not form the normal sp^3-hybrid orbital, but rather sp^2-hybrid orbital [10]. The atom thus forms three σ-bonds in a common plane and the π-bond is directed perpendicular to this plane. This has the effect that the π-conjugation can extend to adjacent branches leading to nonlinear enhancement.

Molecules of this kind are attractive for a number of reasons. We can identify four distinct features that make these novel compounds interesting for the proposed experiment.

1. The high 3PA cross sections due to the efficient π-conjugation in the dendrimers.
2. Large quantum yield of fluorescence facilitates detection.
3. The molecules have a good soluability in polymers and it is thus possible to manufacture samples (films) with high chromophore concentrations.
4. Good long term stability. The molecules are stable and the sample can be used for a long time without degradation or loss of quality.

3 The Laser System

In section 2 it was established (2.1.8) that the rate of excitation for multi-photon absorption is proportional to the peak power rather than the average power. Using high intensity ultra short pulses is therefore very important since it offers instantaneous powers of ~100 GW/cm^2, orders of magnitude larger than any continuous sources. Another advantage of fs pulses is that it can measure the instantaneous multi-photon cross section. With longer duration pulses, the nonlinear absorption can be, and often is, influenced by non-instantaneous processes resulting from transitions from the excited states.

The laser system comprises a Ti: sapphire Kerr mode locked oscillator (Coherent Mira) and a Ti: sapphire chirped pulse amplifier (Clark MXR, CPA 1000). The wavelength region is extended with an optical parametric amplifier (TOPAS, Quantronix).

The oscillator utilities the optical Kerr effect to achieve (passive) mode locking. Initially the oscillator will oscillate in several longitudinal modes in the center of the gain profile. To obtain mode locking, it is necessary to force the laser to oscillate coherently in many modes at the same time. Mode-locking is initiated by a vibrating glass rod placed inside the cavity. The condition that $m \cdot \lambda_i / 2 = L$ thus change and some modes that were oscillating will be suppressed while others that were not oscillating will be enhanced. When the central line is suppressed there is a large number of excited molecules that are forced to oscillate in the other, "allowed", modes.

These modes will randomly form a short pulse every time the different modes oscillate in phase with each other. While passing through the Ti:sapphire crystal this higher intensity pulse will experience self focusing (Optical Kerr effect). Since the Kerr effect is a nonlinear process and proportional to the square of the intensity only the mode locked pulses will experience any significant focusing. By placing a variable slit inside the cavity at the focal point of the Kerr lens one can suppress the CW radiation without affecting the mode locked pulses. The slit thus encourages the laser to work in the mode locked regime. Once a mode locked pulse is formed the system works in a steady state and the rotation of the glass rod can be switched off.

Propagation of a fs pulse through any medium with dispersion add excess chirp to the pulse. Not only the dispersion but also self-phase modulation changes the shape of the pulse envelope. To obtain steady state pulse propagation it is necessary that the pulse envelope

retains its shape after every round trip. This is achieved using a two prism dispersion compensation setup inside the cavity. The prisms generate negative GVD in order to compensate for the positive GVD in the crystal and in the optics. As a result, the oscillator generates nearly transform limited pulses around 780 nm of 150 fs duration at a repetition rate of 76 MHz with an average power of ~400 mW.

The energy per pulse is low (nJ/pulse) at this stage and it is necessary to boost the pulse energy to achieve higher intensity. Amplifying these pulses directly in an efficient way is difficult since it would bring the amplifier close to the damage threshold. To circumvent this problem, the pulses is stretched out in time prior to amplification. This is done in a pulse stretcher, using a diffraction grating. The grating spreads out the spectral components of the pulse in space, such that different frequencies travel different path lengths. The different spectral components exit the stretcher with a small delay relative to each other and the pulse is effectively stretched in time. To achieve large delays the pulses need to pass trough the grating/mirror 8 times (2 full passes in the Clark configuration). The output pulse is typically of 0.2 ns duration and is thus much easier to amplify.

The stretched pulses are then sent to the amplifier. Inside the amplifier there is a Pockels cell that in its "static" position does not affect the polarization of the incoming pulses. After the Pockels cell is a polarizing beam splitter. When a pulse enters the amplifier and no voltage is applied to the cell the pulse will be reflected out before it can interact with the active medium. However, if a $\lambda/2$-voltage is applied to the Pockels cell, then the polarization of the pulse will be rotated so that it will pass through the polarizing beam splitter reaching the Ti:sapphire crystal pumped by a frequency doubled Nd:YAG. After a certain number of passes in the amplifier, the amplifier gain becomes saturated and another $\lambda/2$-voltage is applied to the Pockels cell reversing the pulse polarization, and the pulse is sent out to the compressor.

At this stage the average power has been raised to 1.5 W and the repetition rate has been lowered to 1 kHz. However, the pulses are rather long and compression is needed to bring them back to its original duration. The compressor is essentially a reversed stretcher in that it adds negative GVD to the pulse. Finding the right compression can be a bit complicated and one usually needs to use an autocorrelator and change the amount of compression to minimize the width of the autocorrelation trace. A much more convenient way is to use a multiphoton absorbing material (2PA for 780 nm). Since the rate of 2PA is proportional to the peak

intensity (squared) one can easily see when the compression is at its optimum by observing the resulting up-converted fluorescence. The final output from the CPA system is 150 fs pulses, at 1 kHz repetition rate, with an average power of 0.8 W.

The wavelength tuning of the Ti:sapphire amplifier system is rater limited (~20 nm) and in order to extend the wavelength region a tunable source is necessary. This is done by a process known as parametric down conversion. In this second order nonlinear process, an incoming (pump) photon at 780 nm is converted into a pair of near IR signal and idler photons. This process is widely used to generate coherent radiation in the NIR range. In order for this process to be efficient, both frequency and phase matching conditions must be satisfied. The process is initiated by broadband spontaneous emission called super fluorescence (SFL). If the nonlinear crystal is placed inside a laser cavity, then the feedback from the cavity mirrors amplifies the SFL and laser action can be achieved. This kind of device needs a train of ultra short pulses with a high repetition rate. This means that the amplified pulses cannot be used and the pump pulses will have a low pulse energy leading to a low gain and consequently low energy output pulses. The system used in the present setup is slightly different. If a high intensity pump is used, then even a single pass can generate sufficient gain. Single pass parametric generation is called optical parametric amplification (OPA). The single pass configuration eliminates the problem of pumping of a fs OPO. The main advantage of the OPA is the high output (peak) power. While a typical OPO delivers pulse energies of 10^{-8} J, the OPA in the lab has output pulse energies of ~$80*10^{-6}$ J. Being a high gain amplifier, the OPA has problems of its own. The high gain leads to large fluctuations in output power. Unlike other sources of tunable radiation the quality of the pump laser will determine the quality of the output pulses and any problems with the pump source will greatly limit the performance of the OPA. The lack of a resonator also affects the spatial and temporal coherence properties as well as the pointing stability of the output radiation.

The operation of the OPA is rather complicated and only a brief overview will be given here. When the pump enters the OPA it is divided into three parts, seed, pre-amplifier and amplifier. The seed (first pass) initiates the SFL process while the second pass shapes the broadband SFL by amplifying the collinear components of the seed. The second pass is directed to a diffraction grating. The reflection from this diffraction grating (third pass) overlaps with the preamplifier inside the nonlinear crystal. Since the pre-amplifier is slightly more focused than the third pass a narrower spectrum is selected form the broad SFL. The

final pass, containing the bulk part of the pump, boasts the power of the radiation and leads to the high output power.

The OPA emits pulses of 100 fs duration and pulse energies of 20-80 μJ, and is tunable from 1150-2300 nm. The wavelength region can be extended using different kinds of wave mixing [22].

4. Three-photon Spectroscopy

When studying previous experiments devoted to $3\omega+\omega$ it stands clear that the lack of efficient three-photon absorbing materials has been a serious limiting factor. There exist numerous papers on the subject of two-photon absorption, but the subject of three-photon absorption is up until now largely unexplored. The lack of 3PA measurements is not surprising if one considers the IR intensities needed to make this process observable. For a typical value (not small) of the 3PA cross section, $\sigma_3=10^{-80}$ cm^6s^2, one needs an incident intensity of 30 GW/cm^2 $(\tau = 100\,\text{fs})$ to achieve 10^{-4} % probability of excitation. This is a very high intensity and previous experiments have exclusively used diffraction limited focusing and often using ionization as a very sensitive detection mechanism. This experiment deals with the possibility of imaging $\omega+3\omega$ interference pattern and therefore using extremely tight focusing is not an option. In order to observe a large modulation in the interference pattern one must try to make the probability of one-and three-photon excitation equal. The key issue is to obtain an acceptable signal level, without too tight focusing, so that the detection using a standard camera is possible. This calls for a very special material with a high 3PA cross section. The goal of this section is to find a suitable molecule that is an efficient three-photon absorber in a region accessible with the OPA as well as fulfilling the conditions 1-4 listed on page 16.

4.1 Measuring Three-photon Cross Section

Today there exist two basic methods for measuring multiphoton cross sections: nonlinear transmission (NLT), often referred to as z-scan [23], and fluorescence. NLT is by far the dominating method within this field. The working principle is measuring the actual nonlinear transmission as in equation 2.1.2. The sample is translated trough the focus of a lens and the non linear transmission is recorded as a function of sample position, from which the cross section can be calculated. NLT measures small changes in the transmitted intensity on a large background and it is therefore necessary to use tightly focused beams and high concentration samples. This can lead to problems like thermal lensing, white light generation and (third) harmonic generation. The solvent can strongly affect the measurements at these high powers and the high concentration can lead to aggregation effects.

An alternative method uses multiphoton induced fluorescence, which does not experience some of the problems associated with NLT. It is a zero background measurement since the

fluorescence signal can be separated from the laser light. Modern CCD, photomultipliers or photon counting systems are very sensitive and low levels of fluorescence can be detected. This eases the requirement on high intensity and concentration and makes this method less sensitive to some of the problems mentioned above. The basic idea of the fluorescence technique is to compare the amount of one- to three-photon induced fluorescence [21, 24]. If the one-photon cross section is known, the three-photon cross section can be calculated. This method is attractive since it does not require any additional special equipment (only a spectrometer) and that measuring linear cross section is a standard procedure. The obvious drawback is that the studied compound must fluoresce.

The pulse duration is of great importance in nonlinear cross section measurements. The lifetime of the excited state can be very short, on the order of hundred fs. Once excited, the molecule can relax to new states by charge transfer or intersystem crossing. If the pulse is longer than those relaxation times, there can be a substantial population of intermediate states during the excitation pulse. The pulse (itself) can then excite the molecule to some higher state (both S-S and T-T) which also contributes to the measured nonlinear absorption. These transitions from the excited state can be quite strong, leading to an overestimation in the measured nonlinear cross section. This excited state absorption depends on intensity and it is very difficult to model the influence of the different relaxation processes and deduce the intrinsic cross section.

The mechanisms of excited state absorption have its own applications and are very interesting for optical power limiting [25-26]. It is generally agreed that pulses of ~100 fs duration does not lead to excited state absorption, and are therefore preferred for measuring instantaneous or intrinsic cross sections.

4.2 Experimental Setup for Three-photon Spectroscopy

A number of samples were measured in order to find the best candidate for the quantum interference experiment. All samples are especially designed to have large nonlinear response and they have not been measured before. The samples comprised two different classes of molecules and one BDPADSB /BDPAS dendrimer. One is a class of triphenylamine-branched phenylacetylene dendrimers (OM seies) while the other is a series of linear bis-difluorenylamine-substituted oligofluorenylene-vinylenes (the TFA compounds). The

Chemical structure of the investigated compounds can be found in appendix B. G-0 hybrid and the TFA compounds were synthesized by Prof. Charles Spangler and Dr. Zhiyong Suo, Montana State University. The dendrimers (OM series) were synthesized by Dr. Mirelle Blanchard-Desce, Universit'e de Rennes, France.

A relative method based on fluorescence was used to measure the three-photon cross section for a number of molecules. Making absolute measurements of three-photon cross sections are difficult since it requires accurate measurement of the incident intensity, which is rather complicated since it requires accurate determination of both power and pulse duration. Careful control of excitation volume is also necessary. At the same time, a lack of reliable standards, with well characterized 3PA properties, makes relative measurements difficult. There has recently been an absolute measurement of the molecule BDPAS [24], that will be used as a reference sample in the measurements.

The relative measurements needed to be preformed close to the absorption maximum and only compounds that have similar absorption and fluorescence properties could be measured together. The excitation wavelength was chosen so that it was close to 3 times the transition wavelength of the one-photon transition. The fluorescence detection wavelength was chosen so that a sufficiently strong signal could be collected for all compounds in a series. The samples were thus ordered after their absorption and fluorescence properties into three different series.

The experimental setup for the three-photon absorption measurements is shown in figure 4.2.1. A red-filter was inserted in the beam path to cut off the third harmonic generated in the OPA filters which in turn were used to cut off the pump. A 250 mm lens was used to slightly focus the beam and the sample, a 1 cm cuvett, was placed 1-2 cm in front of the focus. The resulting three-photon fluorescence was collected with a 50 cm spherical mirror and focused on the entrance slit of an imaging spectrometer (Triax 550, Jobin Yvone). The spectra was recorded with a nitrogen cooled CCD (Spectrum One, Jobin Yvone). The focused beam was aligned to be as close to the edge of the cuvette as possible to avoid re-absorption of fluorescence.
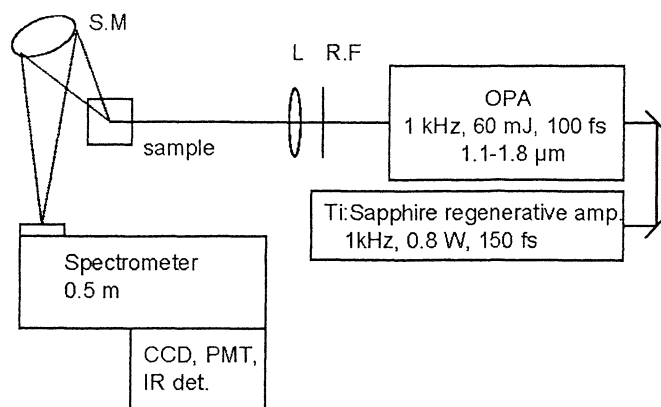
Figure 4.2.1 Experimental setup. R.F=red filter. L=250 mm lens. SM. Spherical mirror.

In this setup, the fluorescence trace is horizontal while the spectrometer slit is vertical. This leads to a lower signal but it has one advantage. It is impossible to avoid third harmonic generation in the optics and in the front wall of the cuvette for high intensity conditions. The (linear) absorption in the sample is high and the unwanted third harmonic will be absorbed over a short distance in the front of the cuvette. The collecting mirror images a small, central, part of the sample (~2mm of 1 cm) and the unwanted one-photon excited fluorescence will not contribute to the signal.

The linear absorption measurements could in principle be made in the same setup. Since all measurements were preformed relative to a standard this is not a necessary requirement. It was more convenient to use the available spectrometer (Perkin-Elmer lambda 900) and luminescence spectrometer (Perkin-Elmer LS 50 B) for absorption and fluorescence measurements respectively.

The samples were prepared by dissolving~ 1 mg of active compound in 10 ml dichloromethane (CH_2Cl_2) and stirred over night. The (linear) absorption measurements were done in a 1 mm cuvette and for optical densities ranging from 0.2-1.8. The extinction coefficients were measured using more diluted (C~10^{-6} M) solutions. The extinction coefficient, $OD = \varepsilon \cdot C \cdot L$, was measured for successively diluted samples to make sure that the sample was fully dissolved. The fluorescence measurements were preformed in diluted (C~10^{-6} M) solutions in a 1 cm cuvette. It is convenient to introduce a relative quantum efficiency of fluorescence (table 4.3.1), which will simplify the three-photon measurements. For diluted samples with small absorption (OD<0.1) one can approximately say that the fluorescence power will be linearly dependent on the optical density. The excitation power was not known but it was the same for all samples. From the measured fluorescence spectra

we calculate the relative fluorescence intensity (at a specific wavelength). By dividing this value by the optical density we obtain a relative probability (per unit OD) that the sample emits fluorescence at a specific wavelength relative to a standard (BDPAS). This value is the relative quantum efficiency η_r.

The three-photon cross section can be calculated from the relation:

$$\sigma_3^r = A\frac{F}{C\eta_r I^3} \quad (4.2.1)$$

where F is the 3PA excited fluorescence count at a specific wavelength (λ), I is the excitation intensity, C is the concentration and η_r is the relative quantum efficiency at λ. A is a constant taking into account non varying experimental parameters.

The three-photon excitation spectrum of three of the compounds were measured. Kasha's rule [27] states that an excited molecule will relax to the lowest lying excited electronic state before emitting fluorescence. The fluorescence spectrum and quantum yield of fluorescence will thus be independent of which electronic-vibrational levels is excited. By changing the excitation wavelength, and measuring the maximum fluorescence count, it is possible to obtain an excitation spectrum that corresponds to the absorption (one-, two- or three-photon) spectrum. The wavelength of the OPA was measured by third harmonic generation and the excitation spectrum was recorded in the same setup as the three-photon cross section measurements.

4.3 Linear Absorption

Figure 4.3.1 a, b and c and 4.3.2 a, b and c shows the absorption and fluorescence spectrum of all samples and the linear spectroscopic properties are summarized in table 4.3.1 a, b and c.

Table 4.3.1a, b,c. λ_{abs} refers to the maximum absorption wavelength, λ_F to the maximum fluorescence wavelength and the value in parenthesis is the excitation wavelength. N_{π} is the number of π electrons, OD is the optical density of the sample, ϵ_{max} is the maximum extinction coefficient, C is the chromophore concentration and η is the relative quantum yield of fluorescence at the detection wavelength.

Name	N_{π}	λ_{abs} [nm]	OD	$\epsilon_{max}[M^{-1}cm^{1}]$ 10^{5}	C [M] 10^{-5}	$\lambda_F[nm]$ (390)	$\eta440$
BDPAS	42	389	12.85	0.53	24.2	455	290
OM67C	52	387	12.08	1.1	11	422	130
OM82C	154	390	11.42	4.5	2.54	460	39.7
OM87C2	358	390	11.04	10.3	1.1	437	47.9
TFA-01	62	376	17.5	0.95	17	428	215

Table 4.3.1 a. Linear data and sample info on the dendrimer series and TFA-01.

Name	N_{π}	λ_{abs} [nm]	OD	ϵ_{max} $[M^{-1}cm^{-1}]$ 10^{5}	C[M] 10^{-5}	λ_F [nm] (390nm)	$\eta510$
BDPAS	42	389	12.9	0.53	24.2	455	70.2
G-0 hybrid	132	424	11.1	2.5	4.4	540	26.8
TFA-02	78	423	3.8	1.06	3.4	512	194.5
TFA-03	94	429	9.1	1.64	3.9	520	186

Table 4.3.1 b. Linear data and sample info of TFA-02, TFA-03 and G-0 hybrid.

Name	N_{π}	λ_{abs} [nm]	OD	ϵ_{max} $[M^{-1}cm^{-1}]$ 10^{5}	C [M] 10^{-5}	λ_F [nm] (370nm)	$\eta430$
BDPAS	42	389	8.4	0.53	15.8	455	512.5
TFA00	42	376	10.4	0.46	22.6	415	279.8
TFA00 hex	42	375	6.8	0.55	12.4	409	142.3
3-arm TFA	45	376	9.9	0.59	16.8	422	412.7

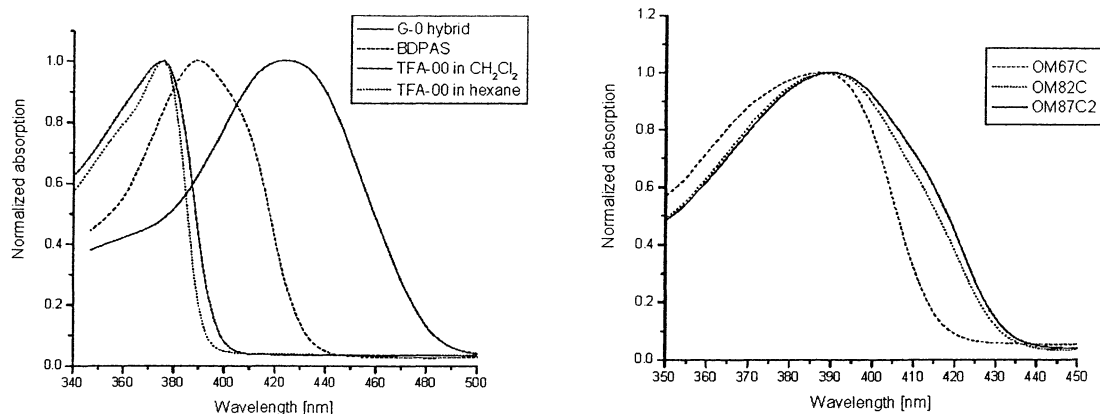*Table 4.3.1.c. Linear data and sample info of the smaller TFA compounds.*

Figure 4.3.1 a. Normalized absorption spectra of G-0 hybrid, BDPAS and TFA-00 (left). Normalized absorption of the dendrimer series (right).
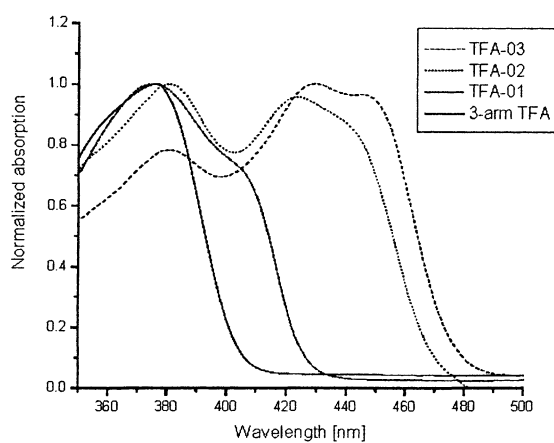

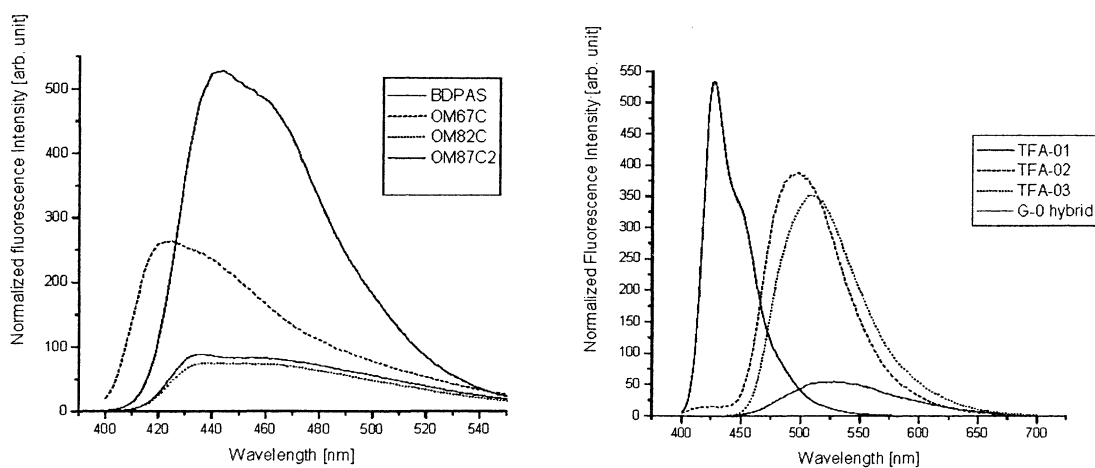*Figure 4.3.1 b. Normalized absorption spectra of the TFA compounds.*

Figure 4.3.2 a, b. Fluorescence spectra of the studied compounds. All values are normalized to the optical density of respective sample.
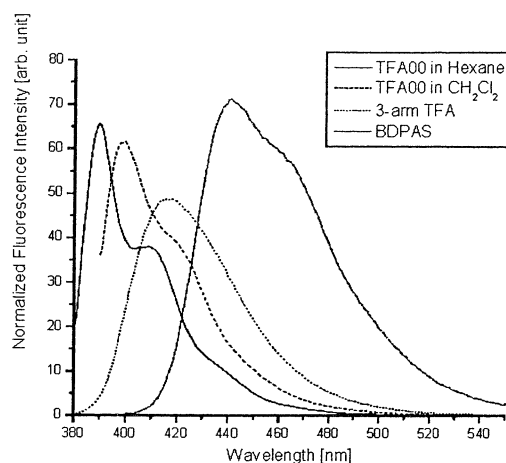
Figure 4.3.2 c Fluorescence spectra of the studied compounds. All values are normalized to the optical density of respective sample.

The linear spectra are all rather broad and show a few distinct features, characteristic for spectra of organic molecules in solution. None of the samples had any linear absorption above 500 nm and it is expected that the S_1 state is the lowest lying energy level in all samples. All compound had a high quantum yield of fluorescence and this also indicates that there are no lower lying states (such as a triplet state).

We note a small red-shift in advancing to higher generation in the dendrimer series. The spectral shape also changes slightly, probably due to new transitions in the higher order series (stronger vibronic transitions). The TFA series behaves slightly different. The red shift in advancing from the smaller molecules (without bridge) to the larger ones is more pronounced. While the lower order TFA's seem to have a smooth spectra, some resolved spectral features can be observed in TFA-02 and TFA-03. This new features probably originates from the extended bridge which is not present in the smaller molecules. The red shift in successive orders is related to the extent of the conjugation and can be understood from a "particle in a box" model. The optically active π-electrons are delocalized and are free to move over a large part of the molecule. When the size of the conjugated molecule increase, then the electrons become even more delocalized. The size of the box in which the electrons can move is roughly proportional to the number of π-electrons. The solution of the one dimensional Shrödinger equation for a potential well with infinite walls give for the transitions frequency:

$\omega \propto (N+1)/N^2$, where N is the number of π-electrons [28]. Thus larger molecules will have a lower transition frequency, i. e. their absorption wavelength will be red-shifted. This red-shift is an indication that the π-conjugation extends over a larger part of the molecules than

the size of the lowest generation. This model works better in the more linear TFA series than in the OM series (dendrimers).

The fluorescence spectra are also broad and rather featureless. All molecules have a large (30-120 nm) Stokes shift and larger molecules have a larger shift than the smaller ones. The shift in these molecules can not be explained by the Frank-Condon integrals as in smaller molecules. The full explanation of this Stokes shift is not known but it has been shown for a molecule similar to BDPAS that the large Stokes shift is due to charge transfer in the excited state. [29]. When the molecule is excited charges migrates from the nitrogen atoms to the core (or bridge), creating a new state that is lower in energy. This process is very rapid and occurs on a timescale of a few hundred fs. Once in this new state, the molecule emits fluorescence and this process can be described in terms of Frank-Condon integrals [27, 30]. The manifold of vibrational and rotational levels gives rise to a broad fluorescence spectrum, much like the more common laser dyes. It is believed that similar mechanisms are responsible for the Stokes-shift in the molecules studied in this work.

All samples but one was dissolved in dichloromethane. TFA00 was dissolved in both dichloromethane and hexane. The solvent has a strong influence on the spectral shape as can be seen in figure 4.3.1.c. The hexane sample has a narrower profile but the transition wavelength is the same for both samples. Generally the solvent will influence both the width of the spectrum and shift the position of the peak. The broadening arises from mechanisms similar to inhomogeneous broadening in crystals. The solvent surrounds the molecules and induces a local field that is different for different molecules and this effectively broadens the transition since different molecules will have different transition frequencies due to this interaction. The interaction with the local field can also shift the energy levels and thus shift the transition frequency. Both shift and broadening is generally larger for solvents with larger (permanent) dipole moments, consistent with the observation in figure 6.2.1.c. [V]

4.4 Three-photon Measurements

To test if the fluorescence signal was due to three-photon absorption a neutral density filter (ND) (T=50%) was inserted in the beam path. For pure three-photon absorption we expect that the fluorescence signal should be proportional to the cube of the incident intensity. All samples showed a drop in fluorescence signal of 7.5-8 indicating pure three-photon excitation (since $1/2^3=1/8$). The fluorescence spectra had slightly different shape on the Triax 550

compared to the luminescence spectrometer. The fluorescence spectra taken in the region where the CCD had a flat response showed that the fluorescence spectra of one- and three-photon excitation were equal.

Linear spectra of all samples were recorded after the three-photon measurements to make sure that no photo induced reactions or decomposition had taken place. TFA-02 and TFA-03 showed a change in the linear absorption spectrum after the 3PA measurement. The exact nature of the change in absorption spectra is not known, but it is probably due to breaking of the double bond (s) in the bridge connecting the two end groups. A new solution was prepared and the samples were measured once again at a lower laser power. This time there was no difference in the absorption spectra before and after the experiments and it is assumed that the sample remained stable at this lower intensity level.

The measurement of series 3 had to be done a slightly off resonance since the maximum transition wavelength of 1110 nm is outside the tuning curve of the OPA [VI] and the available power was too low.

The error in the measurements is mostly due to fluctuations in the OPA output power. This error is estimated to be 30%.

The results of the three-photon measurements are summarized in Table 4.4.1 a, b and c.

Table 4.4.1 a,b,c. λ_{exc} is the excitation wavelength, N_π is the number of π-electrons, OPA Power is the measured output power of the OPA, counts refers to the number of fluorescence counts at the specified wavelength and σ_3 is the value calculated using equation 4.2.1.

Name	λ_{exc} [nm]	N_π	OPA Power	counts @ λ=440 nm	σ_3 10^{-80} [cm^{6}s^2]
BDPAS	1170	42	27	1470	0.5
OM67C	1170	52	25	1408	3.0
OM82C	1170	154	24	1849	62.4
OM87C2	1170	358	24	1357	87.5
TFA-01	1170	62	24	1230	1.3

Table 4.4.1a. Three-photon data of the dendric series and TFA-01.

Name	λ_{exc} [nm]	N_{π}	OPA Power	counts @ λ=510 nm	σ_3 10^{-80} [cm^6s^2]
BDPAS	1230	42	60	827	0.4
G-0 hybrid	1230	132	60	2426	16.8
TFA-02	1230	78	12	1048	5.0
TFA-03	1230	94	12	857	15.6

Table 4.4.1.b. Three-photon data of G-0 hybrid, TFA-02 and TFA-03.

Name	λ_{exc} [nm]	N_{π}	OPA Power	counts @ λ=430 nm	σ_3 10^{-81} [cm^6s^2]
BDPAS	1170	42	24	2585	5.0
TFA00	1170	42	22	256	0.8
TFA00 hex	1170	42	18	47	1.0
3-arm TFA	1170	45	19	452	2.1

Table 4.4.1.c. Three-photon data of the smaller TFA compounds.

4.5 Three-photon Excitation Spectrum

If molecules are centro-symmetric, then the optical transitions can be classified based on parity selection rules. Both 3PA and 1PA are allowed between u and g parity states. However, the cross sections higher dependence on dipole moment makes 3PA more sensitive to electron correlation effects (i.e. conjugation) than 1PA.The situation for two-photon absorption is rather different. The selection rule in this case is g-g and we would not expect to find the peak at the same position in one- and two-photon spectra. If the molecules are non-symmetric, then 2PA g-u transitions become "quasi allowed" and there can be some absorption at the position of the one-photon transition maximum. Multi-photon spectra can thus be used to gain important information about the symmetry of the investigated molecules.

Here we focus only on one-and three-photon excitation spectra and we cannot obtain any information about the molecular symmetry.

Figure 4.6.1 a, b and c shows the three-photon excitation spectrum of G-0 hybrid, TFA-03 and OM87C2 together with the corresponding one photon spectrum. The three-photon spectrum has been normalized to the photon flux thus giving a cross section. The shortest wavelength point in the spectra of OM87C2 is close to the edge of the OPA tuning curve and the power was low, leading to large uncertainty in this measurement point.
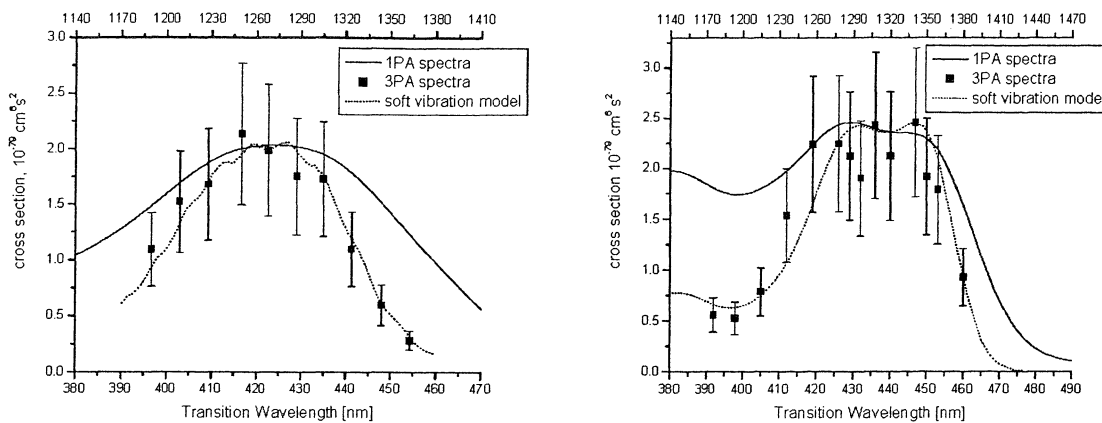
Figure 4.6.1 a and b. Three-photon spectra of G-0 hybrid (left) and TFA-03(right).
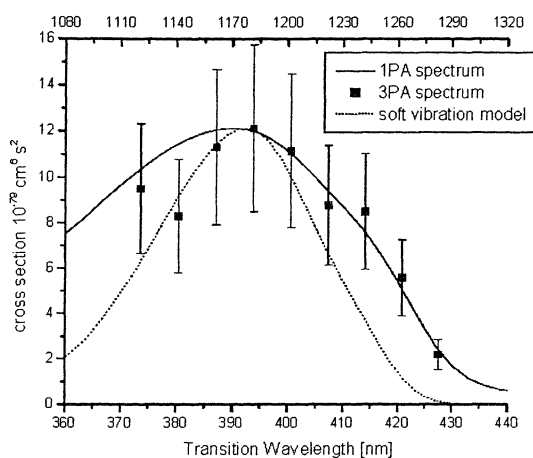
Figure 4.6.1 c. Three-photon spectra of OMC87C2.

The three-photon excitation spectra are very interesting. The peak of the three-photon spectrum corresponds to the one-photon spectrum while the width of the 3PA spectrum is narrower than the corresponding 1PA spectra. The blue part of the all spectra is narrower than the corresponding one photon spectra. In the red tail two are more narrow while one (OM87C2) is not. The present analysis is complicated by the fact that there are very few 3PA spectra published in the literature. Webb et al. [32] have reported that a part of the 3PA spectra in Tryptophan does not follow the linear spectra but the full spectrum was never measured. Two more spectra indicate the same behavior, BDPAS and 4-arm G-2 [21, 24] i.e. that the 3PA spectra is narrower than the corresponding one-photon spectrum. It has generally been assumed that the spectra should be the same, but in these molecules it is clearly not the case. Standard Perturbation theory for multi-photon electronic transitions in atoms predicts identical line shapes for the two different excitation mechanisms for a single, broadened transition. To explain the difference we introduce a new model for 3PA in molecules.

The investigated molecules consists of a large number of atoms (>50). There will be hundreds (3N-6) of vibrational modes that can effectively broaden the electronic transitions. The vibrational modes can be classified as "soft" or "hard", depending on their strength and relative frequency (how they group together). A hard vibration is often broadened by soft vibrations. The electronic spectra can thus comprise a pure electronic transition (0-0 transition) and a number of soft vibrationally broadened hard vibrations. We can identify two limiting cases.

1. The electronic transition is mainly broadened by homogeneous and/or inhomogeneous mechanisms.
2. The electronic transition is mainly broadened by soft vibrations surrounding one dominating hard vibration.

In the first case perturbation theory predicts that the one- and three-photon spectra will have the same shape. In the two-level model, 3PA will scale as the third power of the linear oscillator strength, as shown in 2.1.14. In case 1, one can consider all molecules to have the same oscillator strength. Different molecules have different transition frequencies and the line shape is determined by the number of molecules with each transition frequency.
Therefore, the 3PA spectrum will be also in-homogeneously broadened, with the same shape as the one-photon spectra.

The situation is quite different in the second case. In this case all vibrational (soft and hard) transitions can be considered to be independent of each other. If we assume that the linear spectra consist of a series of partially overlapping vibrations, with a shape of the 1PA spectra, then the 3PA spectra will scale as the third power of the linear spectra. We can thus write for the line shape function (compare equation 2.1.14):

$$g_{3PA}(\omega_{eg} - 3\omega) \propto \frac{g_{1PA}^3(\omega_{eg} - \omega^{TH})}{\omega^4} \tag{4.6.1}$$

where g_{1PA} is the corresponding one-photon line shape function and ω is the frequency of the fundamental radiation.
The model works very well for G-0 hybrid and we see that the three-photon spectrum is narrower on both sides of the maximum. The spectrum of TFA-03 is more complicated to interpret since it clearly consists of more than one dominating transition. The nature of the

two peaks is not yet known. Applying the "soft vibration model" becomes difficult and the plot is done using a mean transition frequency instead of a continuous one, as indicated in equation 4.6.1.

The 3PA spectrum of OM87C2 is narrower on the blue side but follows the red tail of the corresponding one-photon (1PA) spectrum. This case represents a mixture of the two limiting cases. Similar behavior can be seen in BDPAS [21, 24]. The shoulder in the 1PA spectrum indicates that there is more than one transition. If this is the 0-0 transition, then there can be no vibrational broadening on the red side of this transition and this part of the spectrum can be described by case 1. Combining case 1 and 2 thus explains why the spectrum follows the 1PA spectra in the red tail but is narrower on the blue side. Note that the shoulder must not originate from a 0-0 transition for this explanation to hold. The shoulder might well originate from a second electronic transition and if this transition is in-homogeneously broadened, then the same explanation applies.

4.6 Scaling of Three-photon Cross Section

The three-photon cross section of all studied compounds is very large compared to previous measurements using fluorescence technique [21]. The maximum value, $9 \cdot 10^{-79}$ $cm^6 s^2$ is a record large value. It is also interesting to note the large difference between molecules of different size. The cross section varies more than two orders of magnitude from the smallest to the largest molecules, as expected from the stronger influence of the dipole moment.

The three-photon cross sections presented show an interesting scaling behavior. The scaling of σ_3 can give spectroscopic information that is not possible to obtain with linear spectroscopic methods. Linear absorption gives information about the strength of transitions from the ground state. It does not give any information about the strength of transitions from the excited state. This kind of information can be obtained by multi-photon absorption. In the case of two-photon absorption it's also possible to probe transitions that are forbidden in one photon absorption, i.e. g-g transitions.

Recently, a model was presented that predicts the extent of conjugation from linear and three-photon cross sections [21, 24] (referred to as 1-2-3 (photon) spectroscopy). Its main features will be illustrated when analyzing the dendrimer series. Unfortunately, this approach can not be applied fully since the parent molecule has not yet been measured (it is not even synthesized) and that no two-photon measurements has yet been preformed.

The first thing that can be observed from table 4.4.1 is that the cross section grows faster than the number of π-electrons. One finds that the cross section of the second generation dendrimer is ~21 times larger than the first generation, while the number of π-electrons increases by a factor of ~3. The scaling is close to cubic as predicted by the two-level model (equation 2.1.14). If we assume that the first generation is fully conjugated, then we can conclude that the second generation is almost fully conjugated as well. The molecules thus retain its planar geometry. There is an increase from second to third generation but it is not as dramatic as first to second. Determining the size of this π-conjugation in terms of conjugated domains, as proposed [21, 24], is not possible since the cross section for the parent molecule is not known. Nevertheless, we can give an estimate by the following argument. It is likely that the conjugation breaks up into smaller entities of different size and that the main π-conjugated domain should be surrounding the core. We see that an OM82C fits in the center of OM87C2. If we now make the assumption that this part is fully conjugated and that the cross section of an individual "leg" (the parent molecule) is one third of the cross section of OM67C, we can complete our estimation. The total cross section should thus be the core plus the sum of the cross section of the branches. One finds $\sigma_3 = 62.4 + 12 \cdot 1 \approx 74$. This value is lower than the experimental indicating that the actual conjugation of the core is larger than assumed. It seems likely that the core preserves its planar structure but the end legs lose their orientation and twists out of the plane. The twisting of the dendrimer limits the π-conjugation and thus limits the increase of σ_3. The estimation of the conjugated domain is a rough estimate and two-photon data, and independent measurement of the parent molecule, is needed to draw more conclusions. More linear measurements are needed as well to fully characterize the molecules.

The situation in the TFA compounds is more difficult to address. There is a larger difference in the linear spectrum between the different molecules than in the dendrimer series. The spectrum changes its shape and it is shifted ~40 nm going from first to second generation. The first generation spectrum shows more similarity to the spectra of 3-arm TFA and the addition of the bridge seems to be responsible for the shoulder in the one-photon spectrum of the larger TFA's. Comparing the first to the second generation (TFA-01 to TFA-02) is thus not possible since it seems like it corresponds to different transitions. One could compare the long wavelength transition in all TFA's (the shoulder) but the three-photon measurements were preformed at different wavelengths and the scaling of the three-photon spectrum is not

known. Further linear measurements, and three-photon spectrum, are needed to make a statement about the extent of the π-conjugation in this case.

The spectra of generation two and three are more similar and a comment can be made about the scaling. The cross section increases 3 times going from second to third generation while the number of π-electrons in the bridge increases by a factor of 1.5. Again we find almost cubic increase and the whole bridge can be assumed to be conjugated. It can be discussed if it is the number of total π-electrons or only the ones in the bridge that shall be counted. It seems like the end groups are responsible for another transition and does not affect the transition that was measured.

Comparing the measured values with literature values is not straight forward. The numbers of three-photon measurements are limited and all values come with more or less uncertainty. All groups work with "designer molecules" and it is rare that two groups have measured the same molecules. It is interesting to note that z-scan measurements tend to produce results that are higher than fluorescence measurements. The TFA-00 was measured to make an estimate of the difference between the two different methods. A similar molecule (different endgroups, should not change the NL properties) has been measured with z-scan using 35 ps pulses [31]. The reported cross section, $\sigma_3 = 10^{-77}\,\text{cm}^6\text{s}^2$, is far from our value, $\sigma_3 = 10^{-81}\,\text{cm}^6\text{s}^2$. It should be noted that the measurements are preformed at different wavelengths and this can, as we will see, have a big impact on the cross section. The four orders of magnitude difference might seem very large but care must be taken in making any conclusions. 35 ps is a long time long compared to the relaxation processes and excited state absorption is most probably present in the measurements. The cross section was not extrapolated to zero excitation energy so the reported value is not the intrinsic value as measured by us. The concentrations used in those measurements were $\sim 10^{-2}$ M and aggregation effects can occur at such high concentrations, changing the photo-physical properties of the molecule. There are a number of effects that leads to error in z-scan measurements and great care must be taken to make sure that solvent and optics does not compromise the results.

We conclude this section by comparing the cross section of TFA-00 in the two different solvents. The difference is not very large as can be seen in table 4.4.1. The result is not expected to be the same if the local field factor is taken into account. This effect is small (10%), smaller than the error in the measurements. The fact that the one-photon spectrum is different could influence the result as well. It is not an ideal situation to measure at a

wavelength far from the maximum since it is not clear how the 3PA spectrum will scale. The measurements indicate that it should not be any problems in comparing measurements made in different solvents.

5. The Quantum Interference Experiment

It was pointed out in the introduction that most previous experiments on $3\omega+\omega$ interference were carried out in gas-phase and almost exclusively using ns lasers. The relatively low instantaneous power of these lasers leads to a low rate of three-photon absorption and very sensitive detection, like photon counting, has been applied. To increase the signal level, diffraction limited focusing was usually applied. This made the detection of the interference a "point measurement" in space and attempts to make use of the transverse coordinate has never been made. Our experiment differ from all previous ones in several important ways. First, the recent development in novel organic compounds offer nonlinear cross sections that are orders of magnitude larger than that of any molecule previously used for this kind of experiment. This makes it possible to use a much lower degree of focusing and hence opens up for the possibility of imaging the actual interference pattern and even observe it with the naked eye. Secondly, the use of ultra fast pulses probe the instantaneous response of the molecules and it offers much larger bandwidth of the excitation pulses. The main goal of this experiment is to show, for the first time, that $\omega+3\omega$ quantum interference can be produced and detected in an organic solid at room temperature.

However, one can identify a few experimental difficulties that need to be solved in order for the experiment to succeed. The first thing is to preserve as much of the fundamental radiation as possible. This is of outmost importance in order to get a good signal level and facilitate detection. The second thing is to coherently generate third harmonic from the fundamental. The third experimental difficulty is the preparation of the sample. The sample has to be a good three-photon absorber so that tight focusing is not needed. The two pulses will travel with a different phase velocity and consequently change their phase at a different rate. The overlap integral (2.20) will change its value upon propagation, oscillating as a function of distance. What is detected is the sum of the contributions from all positions of the sample and while the two first terms will grow monotonically, the overlap integral will oscillate and thus the visibility will be lower for a thicker sample than for a thin one. In order to observe any modulation it is necessary to have a very thin sample. The coherence length, defined as the (propagation) distance when two waves of different frequencies have acquired a phase difference of $\pi/2$, gives a good estimate of for what sample thickness quantum interference

can be observed. The dispersion is a very big problem in a $\omega+3\omega$ scenarios and the coherence

length $\left(l_c = \dfrac{\lambda}{6(n_h - n_f)} \right)$ is about 3.75 μm in polystyrene [34] $\left(n^f = 1.5695, \; n^h = 1.6245 \right)$.

For propagation distances shorter than the coherence length, the fact that the pulses travel with different group velocity $\left(v_g^f = 1.911 \cdot 10^8 \text{ ms}^{-1}, v_h^f = 1.847 \cdot 10^8 \text{ ms}^{-1} \right)$, and hence eventually run out of overlap, does not come into play.

5.1 Experimental Setup

The experimental setup is shown in figure 5.1.1.
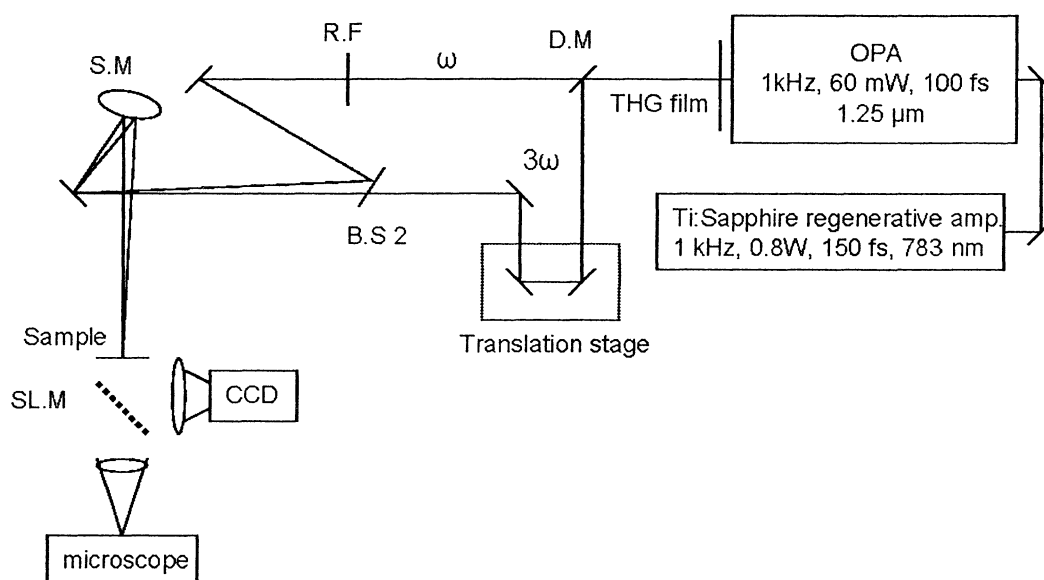
Figure 5.1.1. Quantum interference setup. D.M dichroic mirror. BS2. Broadband beam splitter. R.F red filter, SM spherical mirror f=200 mm, SL.M sliding mirror

The OPA delivered a high intensity infra-red beam with a wavelength of 1245 nm, an average power of 65 mW and approximately 100 fs pulse duration. Third harmonic, at 415 nm, was generated by resonant third harmonic generation in an organic film. The chromphore used for THG was a three-arm G-0 dendrimer based on bis-diphenylamino stilbene (BDPAS) repeat units. The molecule is known to have strong nonlinear optical properties and has been shown to be a good three photon absorber [21]. The chemical structure is shown in figure 5.1.2.

$R_2=O(CH_2CH_2O)_3H$

Figure 5.1.2 Chemical structure of the chromophore in the THG film, a three-arm G-0 dendrimer based on bis-diphenylamino stilbene (BDPAS) repeat units. The subsistent does not change the nonlinear-optical properties but enhances the solubility so that the sample can be prepared as a neat gel.

The addition of the substituents to the end of the arms greatly increased its solubility. In fact, the chromophore became self soluble and formed a neat gel. This gel was pressed between two microscope slides to a thickness to 40 μm. The optical density of the sample was estimated to be ~750 at the transition maximum of 420 nm[**VII**].

The sample was placed as close to the output of the OPA as possible and a strong third harmonic was emitted from the sample, with an estimated efficiency of 1 %.

Constructing an interferometer for both IR and UV radiation required that all the mirrors used were made of enhanced aluminum with a flat reflectivity from 400 nm far into the IR region. The first beam splitter divided the two frequencies into the two different arms of the interferometer. This splitting was not perfect for the fundamental and ~10% was send into the arm with the delay line (UV arm). To remove any TH from the IR arm a strongly absorbing (OD 5+) red filter was inserted into this arm. The second, broadband, beam splitter had ~ 50 % reflectivity for both wavelengths. The pulse energy at the sample was 8 μJ and 0.5 nJ for the fundamental and the third harmonic, respectively.

The two beams were combined at a small angle after the second beam splitter and focused onto the sample to a common ~0.4 mm spot using a 200 mm focal length aluminum coated

spherical mirror. The fluorescence spot, due to one- and three-photon excitation separately, was readily seen with the naked eye [VIII]. The two beams were allowed to intersect at a small angle so that they would give rise to a spatial interference pattern. A sliding mirror directed the light into a CCD camera. When the sliding mirror was removed a microscope ($4\times$ or $10\times$) was used to visually inspect the interference pattern which greatly simplified the experiment.

Images of the interference pattern were recorded with a thermoelectrically cooled CCD camera (PMI 1400 C-12, Xillix, -5°C). The magnification of the standard camera objective was increased by the use of several extension rings. The spatial scale of the CCD image was measured using a calibrated target and the field of view for a 400×400 pixel image was 1.250×1.250 mm. An interference filter was placed in the extension tube to prevent any scattered laser light from reaching the CCD detector. Most experiments were made with the camera detecting fluorescence at an angle but some experiments were made with the camera in transmission mode. It the latter case three filters (2 color glass filters and one interference filter) were used to cut off the strong fundamental.

The molecule of choice for the sample was a four-arm G-0 dendrimer based on bis-diphenylamino di-styryl benzene core (BDPADSB) and BDPAS (bis-diphenylamino stilbene) repeat units. This molecule has a high 3PA cross section, $\sigma_3 = 1.6\cdot10^{-79}\,\mathrm{cm}^6\mathrm{s}^2$, and enough compound was available to produce a few films. Although it does not have the highest cross section compared to the other investigated molecules it absorbs in a region (around 415 nm) where the OPA delivers higher output power (1245 nm). The large Stokes shift and the long wavelength fluorescence (540nm) are also more favorable from a detection point of view. It is also advisable to use wavelengths above 400 nm to avoid large dispersion in the interferometer mirrors. The chemical structure is shown in figure 5.1.3 and it will be referred to as G-0 hybrid in the rest of this work.
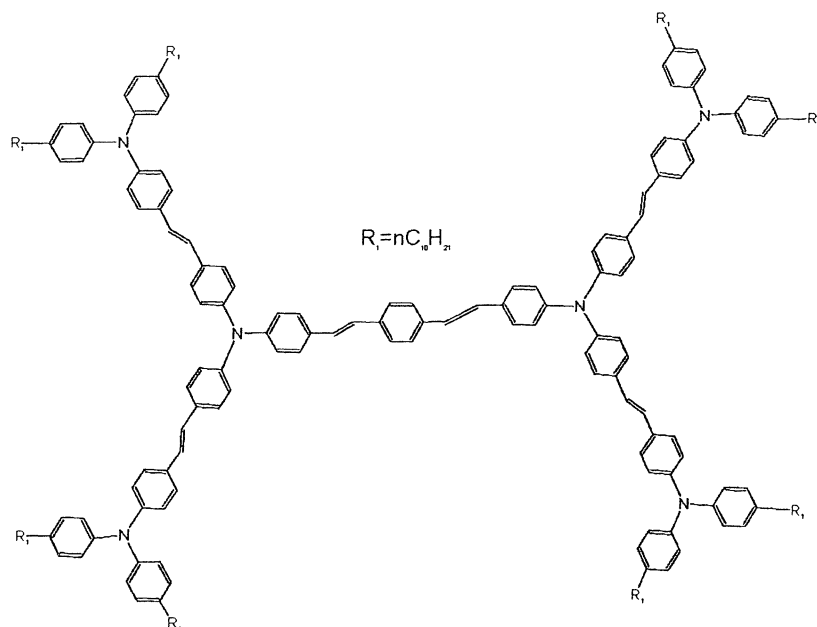
$R_1=nC_{16}H_{21}$

Figure 5.1.3. Chemical structure of G-0 hybrid. The molecule is a four-arm G-0 dendrimer based on bis-diphenylamino di-styryl benzene core (BDPADSB) and bis-diphenyamino stilbene (BDPAS) repeat units

To create thin samples a method known as spin coating was employed. The basic idea of spin coating is very simple. The chromophore is dissolved in a solvent that has a high rate of evaporation. In order to make a film, a polymer solution is added to the mixture prior to the spin coating. If the sample is rotated while the solvent evaporates a smooth thin film will be left on the substrate. The spin coater (Chemat Technology, KW 4A) was kindly provided by Professor C. W. Spangler at the chemistry department at MSU.

~1 mg of polystyrene (PS) was dissolved in 5 ml toluene and a number of tests were preformed to generate a uniform film. If the resulting films turned out to be too thick, then more toluene was added to make a thinner solution. When the solution of PS/toluene produced films of desired thickness, the solution containing the chromphores (dissolved in toluene as well) was added. ~10 drops of chromphore solution was added to ~1 ml PS solution [IX] and spun for 18 seconds at 1750 rpm and for 60 s at 3700 rpm. Absorption spectrums of the samples were measured by a UV-VIS spectrometer in the range 350-800 nm. Figure 5.1.4 shows the absorption spectrum of two of the films.
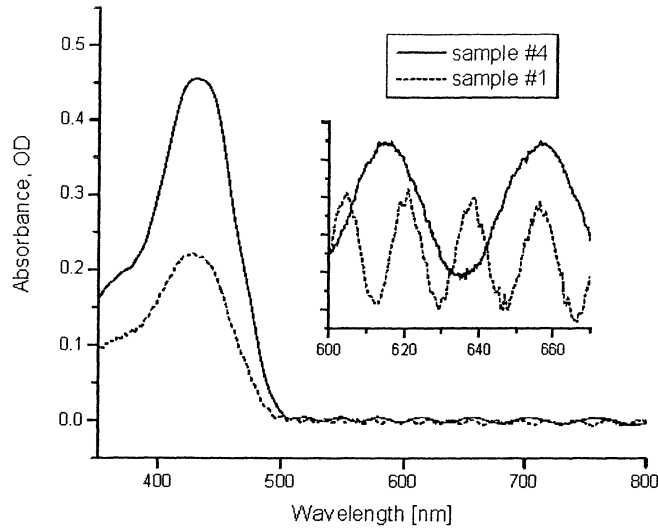
42

Figure 5.1.4. Absorption spectrum of two of the thin films. The inset shows the modulation due to the Fabry-Perot effect.

The modulation of the signal is due to interference between reflection in the front and back surface of the samples, i.e. the Fabry-Perot effect. This made the measurement of the film thickness straightforward. The thickness of the film is given by [35]:

$$d = \frac{k}{2}\left(\frac{\lambda_1\lambda_2}{n_2\lambda_1 - n_1\lambda_2}\right) \tag{5.1.1}$$

where k is the number of periods, n is the refractive index of the polymer and λ_i is the wavelength of peak i in the insert of figure 5.1.4. A number of samples with different mixture of PS/toluene and chormophore solution were made and their properties are summarized in table 5.1.1

Film	OD	T[%]	Thickness [μm]	Concentration [M] 10^{-3}
1	0.22	40	6.9	1.3
2	0.08	83	3	1.1
3	0.22	60	3.2	2.8
4	0.46	35	3	6.1
5	1.35	5	2.5	21.8

Table 5.1.2 Properties of the samples used in the experiments.

5.2 Quantum Interference

The total excitation probability of excitation in $3\omega+\omega$ interference is given by equation 2.2.4. Focusing on the part that will give spatial fringes, thus neglecting wave vector mismatch in the direction of propagation. If one assumes that the two beams fall on the sample at angles θ^{IR} and θ^{UV} one finds:

$$S_{3+1}(x) \propto \int \left[\sigma_3 |F_1(t)|^3 + \sigma_1 |F_3| + 2\frac{\sqrt{21}}{5}\sqrt{\sigma_1\sigma_3 |F_1^{\;3}(t)F_3(t-\tau)|}\cos(\Delta k_{1+3,x}x)\right]dtdz \quad (5.2.1)$$

where $\Delta k_{1+3,x} = 3k_{1,x} - k_{3,x} = 3\frac{2\pi}{\lambda_1}\left(n(\lambda_1)\sin(\theta^{IR}) + n(\lambda_3)\sin(\theta^{UV})\right)$.

For a fixed time delay the cosine function will give rise to a spatial modulation with a fringe spacing of $\frac{2\pi}{\Delta k}$. From the theoretical expression we can further conclude that there will be separate contributions from both three- and one-photon absorption (first and second term) as well as an interference term that is sensitive to the relative phase between the fields. After locating the appropriate time delay separate images of all three contributions were recorded by the CCD camera. The contributions of the regular absorption terms are shown on the top row of figure 5.2.1 while the total contribution is shown on the bottom row. The right image on the second row is a cross sectional cut of the digitized interference image. This image was generated by integrating over a 10 pixel slice in the center of the image.
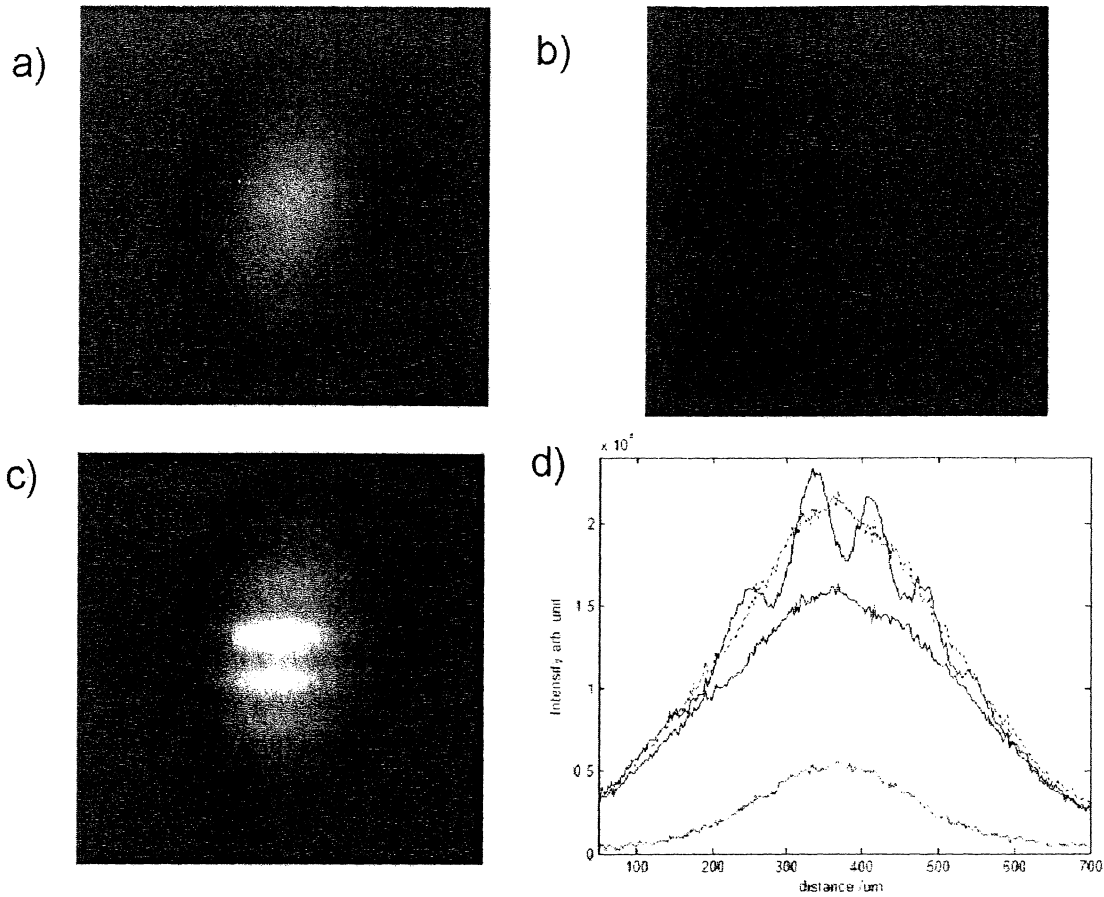
Figure 5.2.1. a) Sample illuminated by third harmonic alone. b) Fundamental alone. c) Interference pattern. d) digitized image of the interference pattern. Image size is 750×750 μm.

The image(c), when both the IR and UV beam are applied simultaneously shows a clear modulation as expected from the modulation term in equation 5.1.2. The effect of tilting the beams with respect to each other gives rise to a relative phase that varies across the sample and this is what turns up as bright and dark fringes in the figure. We can draw one direct important conclusion from the interference image. The fact that we see interference at all must indicate that one- and three-photon absorption takes place between the same initial and final state and we can actually not tell the two processes apart.

The visibility of the fringes are high even if the amount of fluorescence from one photon absorption (1PA) exceed the one from three-photon absorption (3PA) by almost a factor of 3. When comparing the fluorescence due to IR and UV alone it is evident that the fluorescence spot due to 3PA is smaller than the one due to 1PA. This illustrates the higher power dependence of 3PA and if the intensities of the images are normalized to the same value one finds that the spot size of the 3PA image is $\sim 1/\sqrt{3}$ compared to the 1PA image. The conclusion must be that the two beams have approximately the same physical spot size.

45

Another interesting feature is that the pattern extends beyond the apparent dimensions of the 3PA fluorescence spot. Examining the theoretical expression this is not surprising since the interference pattern has lower power dependence than pure 3PA.

5.3 How to Distinguish Between Quantum- and Optical Interference

An obvious question is how to distinguish between quantum- and optical interference. To do so it's instructive to compare different types of interferences that can be studied in the present setup. In the setup we can observe optical interferences like $\omega+\omega$, $3\omega+3\omega$ and quantum interference like $3\omega+\omega$. Figure 5.3.1 shows the interference pattern generated for different time delays. Since the UV pulse will travel with a lower velocity in the second beam splitter, it's necessary to go to shorter delay to observe the $3\omega+\omega$ pattern. The observed difference in time delay corresponded to the one calculated from the difference in group velocity of the IR and UV pulse passing through the last beam splitter. Note that the UV blocking filter in the IR arm of the interferometer makes regular optical interference between two third harmonic pulses impossible. Image 5.3.1a shows $3\omega+\omega$ interference while image 5.3.1b shows $3\omega+3\omega$ interference.
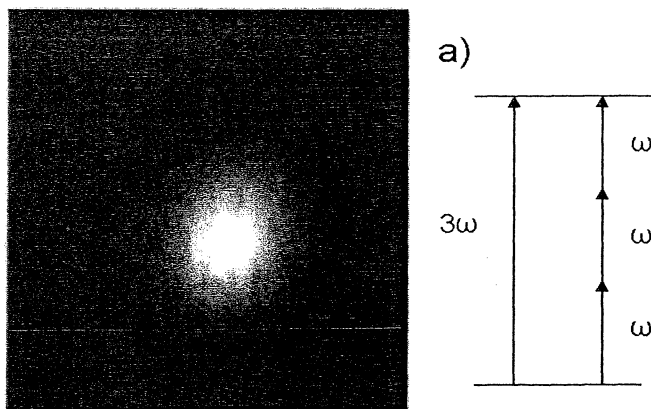

Figure 5.3.1 a Quantum interference via simultaneous one- and three-photon absorption. Image size is $690 \times 690\ \mu m$
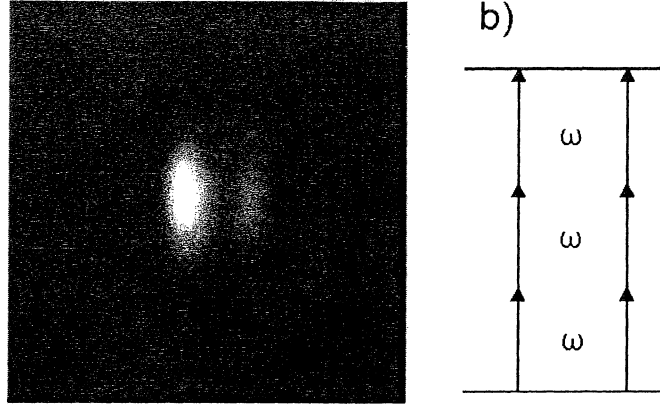
Figure 5.3.1b Optical interference between two three-photon transitions. Image size is $690 \times 690 \mu m$

The quantum interference was discussed in section 2.2. The resulting fluorescence signal for interference between two three-photon transitions can in its simplest form be written as:

$$S_{3+3} \propto \sigma_3 \int \left| \sqrt{F_1(t)} \cdot e^{-i\omega t + ik_1 r} + \sqrt{F_2(t-\tau)} e^{-(i\omega t + ik_2 r)} \right|^6 dt \ (5.3.1)$$

where ω and k is the frequency of the radiation and the wave vector, respectively. Expanding the bracket give rise to a large number of terms. I our experiment the two field amplitudes were highly unequal. The ratio between the two field amplitudes is about 1/20, justifying the approximation $F_2 << F_1$ [X]. The bracket can thus be expanded, keeping only terms with $\sqrt{F_2}$. The two beams cross at a small angle inside the sample and this angular tilt gives rise to a wave vector mismatch both in the direction of propagation and in a plane perpendicular to it. Expanding the bracket, and keeping only terms that will give rise to the spatial interference pattern, one finds:

$$S_{3+3}(x) \propto \sigma_3 \int \left| |F_1(t)|^3 + 3|F_1|^2 \sqrt{|F_1(t)F_2(t-\tau)|} \cdot \cos(\omega\tau - \Delta k_{3+3,x} x) \right| dt dz \ (5.3.2)$$

where $\Delta k_{3+3,x} = k_{1,x} - k_{2,x} = 2 \dfrac{2\pi}{\lambda_1} n(\lambda_1) \sin(\theta^{IR})$ and θ^{IR} is the half angle between the beams

inside the sample. As in the case of quantum interference one finds the fringe spacing of $\dfrac{2\pi}{\Delta k}$ for a fixed time delay.

The $3 \cdot \omega + 3 \cdot \omega$ interference patterns showed a remarkably high visibility. The THG film was still in the setup so the main part of the fluorescence is due to one photon absorption, leading to a large background in the image. The intensities in the two arms were also very different. We see in equation 5.3.2 that there is a strong nonlinear enhancement and good contrast can

be available even if the two fields have very different amplitude. This kind of interference is interesting in itself and can be used for ultra short pulse measurement [37]. It is interesting to compare the two different interference patterns. The $3\omega+\omega$ interference has clearly a smaller fringe spacing compared to the $3\cdot\omega+3\cdot\omega$ case. Since the UV beam is collinear with the IR, the incident angle is the same for the two cases. The angles θ^{IR} and θ^{UV} is to be taken inside the sample and despite the fact that the two frequencies are refracted differently, we find using Snell's law that the ratio of the fringe spacing (equ. 5.2.1 and 5.3.2) for the two cases is always 3.

$$\frac{\Delta k_{3+3}}{\Delta k_{1+3}} = \frac{3}{2}\left(\frac{n(\lambda_1)\sin(\theta^{IR}) + n(\lambda_3)\sin(\theta^{UV})}{n(\lambda_1)\sin(\theta^{IR})}\right) = \frac{3}{2}\left(1 + \frac{n(\lambda_3)\sin(\theta^{UV})}{n(\lambda_1)\sin(\theta^{IR})}\right) = 3 \ (5.3.3)$$

Comparing the fringe spacing in the two cases we find that the ratio of the fringe spacing is very close to 3.

It seems very likely that this is $3\omega+\omega$ interference and the only effect that could be present and give similar result is if the UV beam interferes with third harmonic generated inside the sample (by the fundamental). This kind of interference would give rise to fringes with the similar spacing and it would occur for the same time delay. There is an intrinsic difficulty in distinguish between direct three-photon absorption and third harmonic generation.

To investigate how much TH that is generated inside the sample, we placed a ½ inch pinhole 20 cm after sample in the direction of the transmitted IR beam. Since absorption is low in the sample, we expect that if third harmonic is generated inside the sample in amounts that can excite any fluorescence it should be easily detected with the naked eye. The thickness of the sample is also such that we don't expect a cancellation in transmission due to wave vector mismatch. We were able to observe a very small amount of TH trough the pinhole. The intensity was substantially weaker than the transmitted third harmonic from the THG film. It was, however, comparable to the fluorescence emitted by the sample. Since the third harmonic is coherent and highly directional, while the fluorescence spreads over 4π str, this observation indicates that the third harmonic generated inside the sample was indeed at a very low level, and not intense enough to excite any fluorescence comparable to the fluorescence generated by the external UV beam.

We tried to obtain a more qualitative measure of the TH generated inside the sample by measuring the transmitted TH. The ratio of transmitted third harmonics was 1/60 for an optical density of 0.4. This corresponds to the visual observations. The most powerful evidence that this is not interference between third harmonics is seen when samples of different optical density was measured. The amount of generated third harmonic due to the fundamental alone dropped drastically as the concentration was lowered, while the fringe pattern (in fluorescence) remained unaffected. This demonstrates that this can not be interference between TH and TH from inside the sample, since this process would respond the opposite way, when the concentration was changed ($I_{3\omega} \propto N^2$). This contribution will always be present but we can conclude that it does not play a significant role in our experiment and does not influence our results.

5.4 Dual Color Young Experiment

To better understand the importance and novelty in this experiment we will present below a more detailed comparison a conventional optical interference experiment and our quantum interference experiment. This experiment is often referred to as an analogy to the classical Young double slit experiment but the experiment require a bit more analysis. At first glance, the images (5.2.1) and the equations (5.2.1) do not explain the difference between quantum- and optical-interference. It might even seem like they have similar properties but this is not the case.

Consider a monochromatic beam passing through a Mach-Zender interferometer, shown in figure 5.4.1. Assume that the beam splitters are ideal and broadband and that the light sources have perfect coherence.
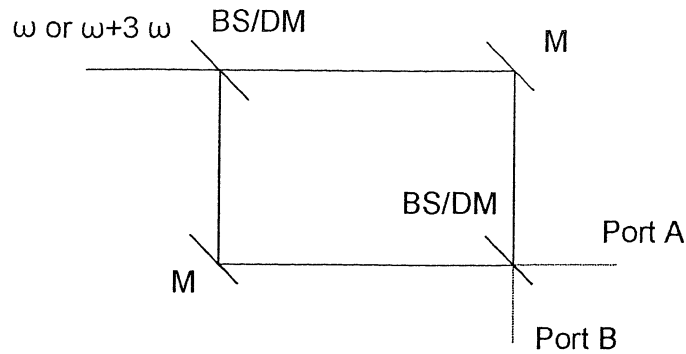
ω or ω+3 ω   BS/DM   M

                                        BS/DM

                                                    Port A

            M

                                        Port B

Figure 5.4.1. Mach-Zender interferometer for an interference experiment. M is a perfectly reflecting mirror while BS is an ideal beam splitter. For a quantum interference experiment one can replace the beam splitters with dichroic mirrors and hence separate the spatial path of the two frequencies.

In the case of one color interference we say that the incoming light travels both paths simultaneously and the recombination on the beam splitter gives rise to interference. According to the famous statement by Dirac [39], "a photon can only interfere with itself", and there is no way of telling which of the two paths an actual photon travel and this is the reason why they interfere. This also means that two coherent beams that pass trough such an interferometer can never be recombined into one beam. If we observe constructive interference on one side of the second beam splitter (port A) there must be destructive interference on the other side (port B). A one color interferometer is thus a "directional coupler" that sends the recombined beam *either* to port A or B depending on the relative phase.

The situation in a dual color quantum interferometer is quite different. If the broadband beam splitters are replaced with dichroic mirrors then the paths appear to be clearly distinguishable. This is the case in our interferometer and there is still interference. To interpret this with the same language as above it is necessary to widen the meaning of the word "path". In one color experiments this is assumed to represent an actual spatial path but this is not correct. From a quantum mechanical point of view, to define a path, one needs to consider the whole process, including the THG and the absorption event. In the case of the same color this does not add to the discussion, since the absorption event is clearly the same, and this part is usually omitted. We see that the fact that photons of different frequencies travel different physical paths does not matter in this case since there will still be two possible paths. From the point of view of the molecule, it is impossible to say if it absorbed one or three photons. Since the harmonic is derived in a coherent process they must be correlated as they are separated in the

We modified the experimental setup to investigate if this transparency effect could be verified experimentally. The camera was moved so that it could measure the transmitted light from the sample. The transmission measurements were plagued by speckle produced by the filters needed to protect the camera from the intense fundamental radiation. Figure 5.4.2 shows an image taken in transmission when the fundamental and third harmonic pulse overlapped inside the sample.
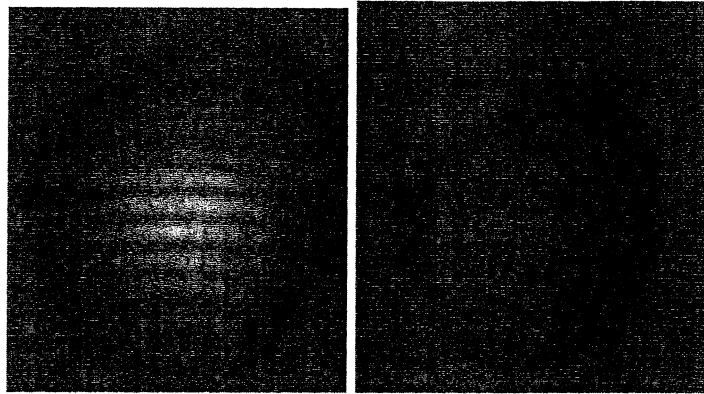
Figure 5.4.2. left: Transmitted TH when the fundamental and TH overlapped inside the sample. right: Transmission of the TH when the pulses don't overlap.

The images (5.4.2) in transmission showed a very clear modulation but this modulation declined rapidly as the optical density was decreased. This is in contrast to what was observed in fluorescence and the conclusion is that the fringes originated from interference (on the CCD) of the transmitted third harmonic and third harmonic generated in the sample. The isolated fringe pattern (patterns – sum of contributions) seemed to be asymmetric around zero. This is not expected for regular interference but this difference was small and it is possible that it originates from variations in laser power.

5.5 Third Harmonic Generation and Quantum Interference

After we have discussed the peculiar effect of quantum interference, it is appropriate to take a closer look at the film that is used for generation of the third harmonic. In section 5.1 it was mentioned that the optical density of the sample at 415 nm is ~750. The thickness of the sample is 40 μm and this gives an absorption coefficient of ~$4.3 \cdot 10^5 cm^{-1}$. The interaction length of the third harmonic generation process will thus be on the order of the inverse absorption length, $1/\alpha$ equal to 20 nm. It seems rather unexpected that 1% conversion

efficiency can be obtained for such a short propagation distance. The short interaction length should produce a beam with large divergence but this it not the case. This behavior can not be explained by a simple model for harmonic generation.

It seems like the answer to these question can be found in the effect of quantum interference. A number of theoretical papers have been published on the enhancement of photo ionization by quantum interference in gas phase [18, 41-44]. These theoretical models indicate that the generated third harmonic is generated such that it is out of phase with the driving field and that the two fields interfere by $3\omega+\omega$ interference and cancels absorption of both fundamental and harmonic. This has been demonstrated in experiments with resonant ionization in atomic vapors (see references in 40). Quantum interference can thus lead to a "soliton like" [XI] propagation of the two fields. An interesting feature is that the third harmonic envelop will be proportional to the cube of the fundamental leading to a shorter pulse duration. All theoretical papers have assumed dispersionless media and the effect of dispersion in this process is not known.

None of the above effects have been observed in the condensed phase and a number of experiments need to be preformed in order to determine if this is what is happening in the THG film. One should try to measure the real pulse duration of the third harmonic in a better setup (see discussion in Appendix A.3/A.4). This should show if the third harmonic actually is shorter than the fundamental. A second experiment would be to try to image the fluorescence trace. It is not clear if the mechanism is continuous generation and re-absorption or if the pulses "lock" together and propagates without affecting its surrounding. An image of the trace would resolve this question. The perhaps simplest experiment is to make a thicker film (on the order of a few mm at least). For longer propagation distances the group velocity mismatch becomes very important. The fundamental pulse is faster than the generated pulse and the harmonic pulse will be stretched and may actually acquirer a more complicated shape. It would be interesting to see how a thicker film affects the shape and duration of the generated third harmonic.

5.6 Qualitative Measurements of the Fringe Pattern

The discussion in the previous section indicates that our theoretical model can not describe this phenomenon very well since it does not take into account any interaction of the field and the molecules. We here base our discussion on a simple model, where we treat the fields and the molecules independently from each other. What is really going on is difficult to say from this simple model and research papers, and it is not that obvious that absorption and refractive index behave like they do in the normal case. Only few studies of quantum interference has been reported so far and therefore it is of interest to see if this simple model can describe some of the properties that can be measured readily.

The theoretical expressions (5.2.1) for the quantum interference pattern indicate that the power dependence of the interference pattern alone should be lower than for pure three-photon absorption. This is indicated in figure 5.2.1 as we see that the interference pattern extends beyond the apparent spot of the 3PA image. A more systematic measure of the power dependence was made by placing a density (ND) filter in the IR-arm of the interferometer. [XII]. Varying the optical density of the ND filter made it possible to measure the power dependence of the fringe pattern. Figure 5.6.1a show the normalized fringe amplitude as a function of the excitation power.
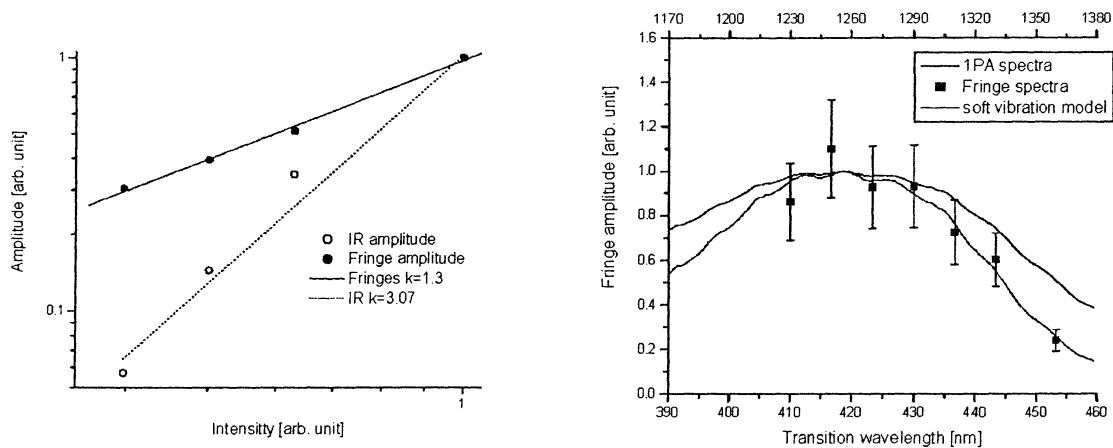

Figure 5.6.1 a and b. (left) Power dependence of the fringe amplitude and the maximum value in the 3PA images. (right) Fringe amplitude as a function of wavelength.

Also shown is the power dependence of the pure 3PA image. The slope in the log-log plot is 1.3 and 3.1 for the fringe amplitude and pure 3PA, respectively. The number of points is low but it seems like the power dependence fall in the range predicted by theory.

It is not possible to factor out the individual cross sections from the mathematical expression (5.2.1) (as one can for optical interference) and a measurement of the "interference pattern spectrum" would be interesting since we found in the spectroscopic measurements that the 3PA spectra was different from the 1PA spectra. Figure 5.6.1b shows the variation of fringe amplitude as a function of wavelength. The "spectrum" is clearly narrower than the one photon absorption spectra. In section 4 we saw that the 3PA spectrum is narrower in G-0 hybrid and scaled as the third power of the one photon absorption spectrum. A fit using the square of the one photon spectrum shows a good agreement with the experimental results.

An interesting question is the visibility of the fringe pattern. One can imagine things that will affect the visibility such as the overlap between the pulses, the relative excitation probabilities, thickness of the sample and the optical density of the sample. To be able to make any qualitative measurements it is necessary to define a measure of the visibility. We define the visibility of the fringes as:

$$V = \frac{I_{max} - I_{min}}{I_{max} + I_{min}} \quad (5.6.1)$$

For the image (5.2.1) in section 5.2 we find that the maximum visibility in the center of the image is about 14 %.

One important circumstance that will affect the visibility is the fact that the two fields will propagate differently inside the sample not only because they have different group velocity but also since they are absorbed in different ways (section 1). The intensity of the third harmonic experiences attenuation and decays as an exponential function while the intensity of the fundamental can be considered, to a very good approximation, to be constant over the entire sample. If the sample has too high optical density, then the probability of excitation across the sample will be very different for the two mechanisms and the visibility will, consequently, decrease. Separate images of the different samples in table 5.1.1 were recorded to determine the influence of this effect. When the optical density goes down, it was, unfortunately, necessary to increase the integration time of the CCD camera to maintain a good signal to noise ratio. This affects the measured visibility and it is expected to go down for longer integration times due to vibrations and low pointing stability of the beams. The

measurement will under any circumstances give a rough idea about the magnitude of this excitation mismatch and its effect on the visibility. The results are summarized in table 5.6.1.

Film	OD	Thickness [um]	Integration time [s]	Visibility [%]
1	0.22	7	60**	1.5
2	0.08	3	110	8.8
3	0.22	3.2	40	11.5
4	0.46	3	30	11.5
5	1.35	2.5	15	7.8

*Table 5.6.1. Visibility as a function of the optical density for the different samples. ** indicates that the images were taken in a different geometry and under different conditions.*

As expected, the visibility was clearly lower for the high optical density sample. There seemed to be an optimum optical density between 0.2 and 0.4, but this is probably due to increased integration time. The optically thinnest sample does not show the best contrast, which confirms the suspicion that other mechanisms strongly affect the visibility for longer integration times. The change in integration time between sample 2 and 3 is not very large and we can assume that the visibility has a weak slope in the region from 0 to 0.4 (OD) (in this setup).

Another parameter that intuitively should have impact on the visibility is the ratio of fluorescence of one and three-photon excitation. When the focusing condition was changed and the pattern was observed visually, then no difference in visibility for different focusing conditions could be observed. This was examined more systematically with the CCD camera. A number of different images under different focusing condition were recorded and analyzed in the same way as image 5.2.1. Figure 5.6.2 shows the fringe visibility as a function of the ratio F_{IR}/F_{UV} in the central slice of the image. The variation between two consecutive images was rather large (the laser had a bad day) and the error bars indicates an $\pm 1.5\%$ error, approximately the standard deviation of a series (4 images) taken under the same conditions. The visibility does not change very much for different ratios. When comparing the left part with other measurements done at different times (example figure 5.2.1) it seems like this side is lower than expected. The exact functional dependence is not of interest but it is very interesting to note that the visibility is more or less independent of the fluorescence ratio over a broad region from 0.5 to 1.5.
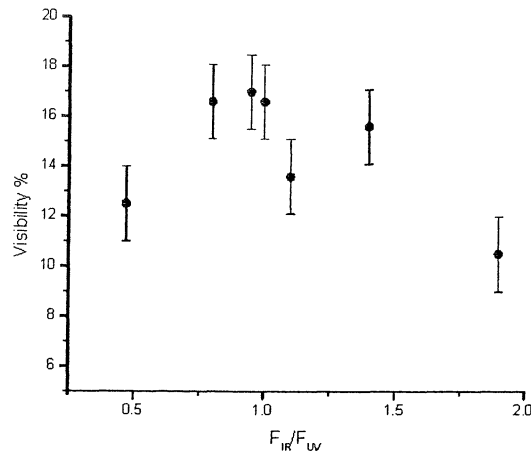
Figure 5.6.2 Visibility as a function of the ratio of 1PA- to 3PA-fluorescence. Error bars indicate a 1.5 % error.

The flat response of the visibility indicates that there are other parameters that are more important in limiting the visibility. When measuring the duration of the pulses by auto- and cross-correlation it was found that the third harmonic was broader than the fundamental (see Appendix A for technical details) and that the pulse duration was 70 fs and 110 fs for the fundamental and third harmonic respectively. To estimate the effect of changing the pulse duration of one of the pulses a glass plate was inserted after the interferometer. The trace broadened by 50 fs and this should be exclusively due to broadening of the UV pulse. The visibility of the fringes did not change significantly. It was difficult to analyze the results since the residual reflection from the glass plate changed the relative ratio of fluorescence (due to the higher power dependence of 3PA). When the fluorescence ratio with and without the glass plate were in the region where the visibility is independent of the ratio only a small difference of 1 % could be detected. This difference was on the order of the standard deviation of five consecutive images. This seems counter-intuitive since broadening of one pulse should lead to worse overlap and thus lower visibility. This is generally true but a more careful examination of the pulse overlap is needed to explain the results. The fundamental enters the overlap integral to the third power and this means that the effective pulse duration is shortened by a factor of $\sqrt{3}$ (for Gaussian shape). One should thus compare this "effective" duration to the duration of the third harmonic. A requirement for this pulse shortening is that the absorption profile can support such pulse shortening. In our case the FWHM ratio of spectral width to absorption width is 1/5 and it seems like it is possible to assume that the effective pulse duration of the fundamental is shorter.

With this effect included we find that the effective durations are ~50 and ~110 for the fundamental and third harmonic, respectively. The overlap integral is dominated by the fundamental when the difference is large. Extra broadening of the third harmonic does not affect the visibility of the images in this regime as we see experimentally, since the overlap integral has approximately the same value with and without extra broadening.

The largest reason for lack of visibility is probably due to the influence of sample thickness. In a thick sample the integrated interference pattern will lose visibility due to the phase-and group-velocity mismatch. We would therefore expect that a sample with a thickness on the order of twice the coherence length, l_c would give almost zero visibility. Two different thicknesses were available, 3 and 7 μm and with different optical density, OD=0.4 and OD=0.22. The coherence length for a $3\omega+\omega$ interaction in polystyrene is about l_c= 3.75 μm. The thin sample gave a visibility on the order of 14 %, in line with the previous measurements. The thick sample produced an image with substantially lower visibility. The digitized images showed a visibility of about 1.5 %. So small modulations are hard to measure since the detection noise comes into play. The excitation conditions were slightly different but it clearly demonstrated the influence of sample thickness. It is interesting that the thick sample generated images with visible fringe pattern. One would expect that the visibility would be even lower than the measured value. Since absorption of the third harmonic changes the local probability of excitation one can not consider that all parts of the sample contribute with equal amounts to the overlap integral. The predicted cancellation of the integral will not be complete and a small fringe pattern is still visible. Strictly speaking, one can not neglect the influence of the wave vector mismatch in the direction perpendicular to the propagation direction (x-axis). The fringes will be slightly shifted for different positions in the sample. The full integral will thus be of sine function with a gradual displacement from the x-axis. This is a small effect compared to the wave vector mismatch in the direction of propagation.

What is then the maximum visibility? This is indeed an interesting question for any potential application. We have seen that there are many reasons for loss of visibility. The combined effect of rotational averaging and sample thickness seems to be the major reason for loss of contrast. An evaluation of equation 2.2.4 is shown in figure 5.6.3 for a three dimensional sample with spatial fringes (i.e. wave vector mismatch in a direction perpendicular to the propagation direction). The pulses are assumed to be of the same duration and absorption of the fundamental has been neglected.
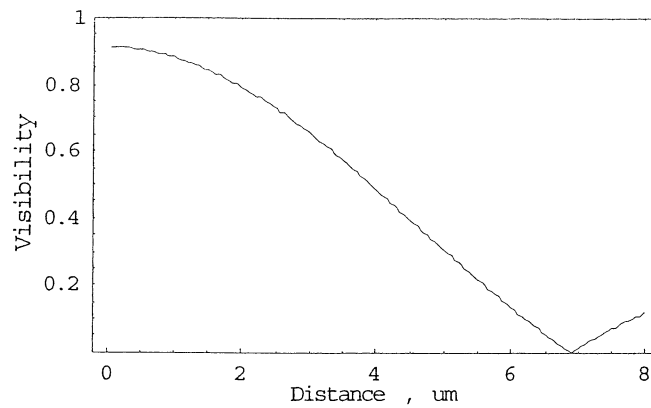
1

0.8

Visibility

0.6

0.4

0.2

0   2   4   6   8

Distance , um

Figure 5.6.3 Fringe visibility vs. distance.

The maximum contrast is only ~65% for a sample of 3 μm thickness. We see that the visibility drops rapidly as a function of distance. This is expected since the two first terms grow monotonically (low absorption) while the interference term oscillates and will "drown" in the separate contributions. The discrepancy between the model and the experimental results is very large and it is difficult to explain this results. We realize that different pulse durations will significantly decrease the visibility. We can estimate this effect by evaluating equation 4.2 for an infinitely thin layer with the pulse properties measured in section A.4. We find that the maximum contrast in this case is 68 % and this would mean that the maximum contrast for a 3 μm sample would be on the order of 50%, if we neglect the changes in the pulse shapes as the pulses propagate. This is still far from our experimental results and there seems to be something with the experimental setup that limits the visibility. Visual inspection of the fringe pattern indicated that vibration in the interferometer was not a big problem, i.e. the fringes were stationary. The visual inspection revealed another fact that limits the visibility. The beams had rather poor directional stability and this movement becomes noticeable when the beams are focused. The illumination is not uniform during the whole exposure and the fringe pattern becomes smeared out. The asymmetry mentioned in connection to the pulse measurements is also a factor that will affect the results. The last point about this subject should be about the resolution of the camera. Most pictures were taken under conditions corresponding to 10 pixels per fringe. This should be enough resolution but it can not be excluded that the resolution (and focusing) affected the results.

6. Conclusions

Quantum interference in an organic solid has been demonstrated for the first time. The fluorescence image show a clear modulation when the sample, comprising a thin polymer film activated with a special organic molecule, is illuminated with a strong fundamental beam and the harmonically derived third harmonic. The visibility of the fringes is about 15 % and the interference has a high degree of spatial confinement, on the order of the coherence length. It is shown that the visibility of the fringe patterns is sensitive to both the concentration of the chromophore and to the thickness of the sample but, for the current experimental settings, remarkably insensitive to small changes in the excitation probabilities and broadening of the third harmonic pulse.

The experiment demonstrates that one- and three-photon transitions occur between the same initial and final states, shredding any doubt induced by the sum over states expression for the three- photon cross section. It also serves as an analogy to the classic Young double slit experiment and the similarities and differences have been discussed. The main difference is that two color interference is a single port interferometer. While ordinary interference can be observed under quite general conditions one needs a special "detector" to observe this quantum interference. A spectroscopic study was made to find a molecule that constituted a suitable detector and the three-photon cross sections of two classes of π-conjugated molecules were measured. The different series both show cooperative enhancement and it is concluded that the π-conjugation extends over almost the entire molecules. The large extent of the π-conjugation leads to large cross sections, where the largest, $\sigma_3 \approx 1.2 \cdot 10^{-78} \, cm^6 s^2$ for the largest dendrimer, is a record large value when compared to previous measurements using fluorescence technique. Three-photon spectra for a number (3) of molecules have been recorded and it has been shown that the spectral shape deviates from the one predicted by perturbation theory. A new model, the "soft vibration model", has been introduced to explain the experimental results.

The visibility of the interference pattern could be improved by changing the setup so that the third harmonic only experiences reflections and thus avoids the broadening associated with passage through an optical component which turned out to limit the visibility of the interference pattern in the experiment. Another way to improve visibility is to prepare a thinner film. More experiments and theoretical modeling is needed to gain more knowledge

about this kind of interference, both in thin film and from point of view of large scale propagation (resonant third harmonic generation in material with high three-photon cross-section).

Notes

I. The quantum interference described by Manykin is only a "special case" of the chemical interference described above. To see this consider the following situation. Assume a molecule with two degenerate energy levels corresponding to two different scenarios (dissociation, state 1 and ionization, state 2). The two states will have different wave functions and there will thus have different transitions dipole moments and consequently different transition rates. The two states are independent and we can consider two two-level cases. Both cases will show quantum interference and thus show a variation with the relative phase of the driving fields but the modulation depth will be different for state one and two (the ratio

$$r_i = \frac{\sigma_1 I}{\sigma_3 I^3}$$ will be different, see equation 68 in ref 5 for more details). The total transition rate (for both

two-level models together) will show a modulation since each path will change differently when the phase is changed (different mod. depth for the two cases). A change in the phase of the driving fields will thus lead to a larger suppression for one of the states relative to the other and its possible by changing the relative phase to enhance (or suppress) a certain outcome. The key issue is the larger difference in transition rates for higher order transitions.

II. It might seem strange to talk about infinite times when dealing with fs pulses. The sinc-function is rather peaked and we can neglect the side wings and say that the main contribution will come from the central part. From the uncertainty principle we find that the "absorption time" is inversely proportional to the line width. For the molecules in this paper we have $\Delta v = 1.2 \ 10^{14}$ Hz and the absorption time will be on the order of a few fs. For more on this subject, see [2]. A more complete description of the light matter interaction in the Bloch equations show that the rate equations are valid when the de-phasing rate is larger than the rate of change of the normalized electric field amplitude.

III. The full expression contains the third order temporal coherence and the local field factor as well. These factors are small and in cases difficult to determine experimentally with any accuracy (the coherence). The local field factor will be of interest when comparing results in different solvents but the difference between different solvents are smaller than the accuracy of the measurements and we will omit it for the rest of this paper.

IV. One and two photon transitions do not take place between the same initial and final states in the first approximation. The selection rules are g-u and g-g respectively. The g-g selection rule can be relaxed if the transition contains symmetric vibrations. These "forbidden" transitions can be observed but are generally weak.

V. Dichloromethane has a small dipole moment while hexane is virtually non polar. No values are given here since most tables don't list the dipole moment of hexane since it's so close to zero.

VI. This is not strictly true. The 1000-1150 nm region is difficult to reach. The best bet is to use second harmonic of idler but this region (2200 nm) is on the edge of the idler tuning curve and the process will not be very efficient. For the measurement of spectra this is however not a good idea since there is no guarantee that the signal and idler pulse widths are the same.

VII. The absorption spectra of the THG film is not shown since it was distorted due to saturation of the detector. The spectrum is broad and centered around 430 nm. A spectrum of the chromophore in dichloromethane can be found in [24].

VIII. From the measurement of the spot size, pulse energy and pulse duration it is possible to estimate the amount of fluorescence. Taking 400 um, 8 uJ and 70 fs and a concentration of $6 \ 10^{-3}$ M one finds that the probability of excitation is about $4 \ 10^{-4}$ and that the number of ecxited molecules is about $2 \ 10^{11}$. The quantum yield of fluorescence is about 90% while the collection and detection efficiencies are 2% and 10 % respectively. The total collected fluorescence is on the order of nW or 10^9 photons per second.

IX. The exact concentration of the solutions used for spin-coating is not known. The values given are starting values and are approximately correct. A trail and error method was employed and the exact concentration was not of interest. More chemicals were added until a "good" film had been manufactured.

X. The fringe spacing will not be affected by this approximation but the peaks will be narrower. Compare to coherent addition in multiple slit diffraction.

XI. It is not strictly a soliton since it is not a stationary (or periodic) solution to the nonlinear Schrödinger equation. Clear is that the UV pulse will not experience the broadening it would without the IR and the pulses will not separate as one would expect but what really happens is not known since the effect of dispersion in this kind of propagation has not been addressed.

XII. This is not an ideal solution since the different filters may affect the width of the pulse in different ways. A better solution is to use two polarizers and by changing the angle vary the excitation power. This is however not a big problem and it should be negligible compared to the variations in excitation power.

APPENDIX A

Technical Details

This appendix covers further details about the experiments that did not fit in the main text. These details are important to show that a variety of possible scenarios have been considered that may influence the results. A person who would like to redo the experiments might find this section very useful as well. Although they are nice and important experiments they might confuse the reader about what is really important and the volume and detail might hide what is really novel.

A.1 Third Harmonic Generation in the Spectroscopic Measurements

It should be clear that third harmonic generation in the cross section measurements is a major problem leading to the question about what is really being measured. Lack of transmission of third harmonic does not mean that this process can be neglected since the sample will absorb strongly at the third harmonic wavelength. The first step to minimize the influence of third harmonic induced one photon absorption is to use a solution with as low concentration as possible since the two processes have different concentration dependence. However, one must remember that all materials generate third harmonic and the influence of the solvent must not be neglected. The third order polarizability of a small molecule (solvent) is generally very low ($\sim 1.5 * 10^{-36}$ esu. for dichloromethane) but it is present at a high concentration in the sample. In our experiments the concentration of the solvent is roughly six orders of magnitude larger than the concentration of the sample molecule. Even if the third order polarizability of the solvent is orders of magnitude lower than the sample we see that the susceptibility $\left(\chi^{(3)} = \langle \gamma \rangle N\right)$ is larger. It is a good approximation to neglect the third harmonic generated by the sample molecules and concentrate on the third harmonic generated by the solvent. This allows a separation between the two processes and one can try to measure the transmitted third harmonic generated by the solvent alone. The solvent was transparent in the region of interest and there will be no re-absorption and one can see this third harmonic on a piece of paper after the sample containing pure solvent. Observing this third harmonic after the sample was very difficult since it is comparable to the fluorescence emitted by the sample. The total optical density of the sample was ~ 15 and one would expect that a large part of the generated third harmonic will be reabsorbed. When observing the third harmonic generated by the

solvent some care must be used when applying equation 2.3.2. The equation is derived for a CW field and the effect of pulse propagation becomes important for longer propagation lengths. The separation length, i.e. the length when the two pulses are separated by a time equal to their duration, is on the order of 2 mm in dichloromethane (100 fs pulses, The dispersion of dichloromethane is not known. Ethanol, with similar absorption spectra, has a separation length of 2.5 mm. These solvents are not very dispersive in this region (far from resonance) and the separation length in polystyrene is only 0.9 mm). What happens in this case is that the third harmonic pulse will be stretched out since the fundamental, that moves faster, will generate ahead of the third harmonic pulse. This also makes the cancellation effect (compare with phase matching) less important since parts with different phases don't overlap in time. This effect will make phase mismatch less important in this case compared to the CW case and we would expect that there can still be third harmonic even with a large wave vector mismatch. This kind of pulse propagation becomes very complicated and it is not easy to predict the exact shape of the generated pulse. We are only interested in the amount of fluorescence that the third harmonic can produce and since one photon absorption is proportional to the average power, we don't need to consider the pulse shape. The fact that one can see third harmonic after the sample indicates that there is some truth in the explanation above. There seemed to be no difference in the transmitted third harmonic as the sample is tilted i.e. the sample length was changed, indicating that phase mismatch is not that important. It is clear that adding absorption will change the way that third harmonic is generated but there is little hope to address this question in another way.

The amount of third harmonic generated by the solvent was measured using a power meter (Molectron J3S-10). Since the third harmonic was collinear with the strong fundamental three blue filters (OD~10) was used to cut off the IR radiation. Attempts to measure the third harmonic pulse energy failed since the power was to low too be measured by the power meter. Not even when focusing was on threshold of white-light generation could any third harmonic be detected. We assume that the pulse energy is at the detection limit of $5.48*10^{-12}$ J. This is an absolute maximum since it includes third harmonic generated in the back wall of the cuvette. The optical density of the samples was ~15 and the sample length was 1 cm. This means that most of the generated third harmonic is absorbed over a distance of 1 mm (97%). To compare the amount of fluorescence generated by third harmonic and 3PA a 1 mm cuvette with the sample (G-0 hybrid OD~1.2, $\sigma_3 = 10^{-79} \, cm^6 s^2$) was placed in front of the CCD in the quantum interference setup. The power and focusing of the fundamental was controlled so

that it corresponded to the settings in the fluorescence setup. The third harmonic generating film (THGF) was used to generate third harmonic that was used to excite the sample in the thin cuvette. The total amount of fluorescence was compared to the 3PA generated by the fundamental by integrating over the both images. The power meter was used to measure the power of the third harmonic (from the film) and this value was compared to the one measured using the solvent alone. We assume that the pulse energy grows linearly with propagation distance and we shall thus compare 1/10 of the pulse energy from the solvent measurement (1 cm cell) to the energy measured when using the THG film for excitation.

The integrated fluorescence under these conditions scaled as 8.8 for excitation power 30 mW (fundamental) and a (fluorescence) spot size of the 3PA spot of ~0.5 mm (FWHM). The pulse energy of the light used for 1PA form the THG film was 82 10^{-12} J. We thus find that the fluorescence generated by the third harmonic from the solvent is $8.8 \cdot 82 \cdot 10/5.48 \approx 1300$ times less than the fluorescence from three-photon absorption. We must remember that this is a simple model based on a number of assumptions. It is very complicated to judge if the model predicts a true value. The obtained value of third harmonic is probably a higher estimate since we could not measure the real value but rather use the limit of the detector and this measurement includes third harmonic generated in the back wall of the cuvette.

We can thus conclude that third harmonic induced one-photon absorption did not effect our measurement of the cross section, not even for the smaller molecules. For this kind of concentrations and cross sections we find that the pure 3PA is much stronger than the process of third harmonic generation and one-photon absorption. The processes have the same power dependence and it seems that the requirement that the cuvett (the glass) must not generate third harmonic is sufficient to guarantee that 3PA is by far the dominating process as long as the cross sections is larger than $\sim 10^{-82}$ cm^{6}s^2. It is interesting to note that this estimation is in good agreement with the one made by Cable et. al [33], who found that pure three-photon absorption dominated by a factor of five in benzene(with $\sigma_3 \sim 10^{-82}$ cm^{6}s^2). Their estimation was based on comparing one- to three-photon fluorescence of two molecules in a mixture. In the literature one can find lower cross sections than this and the question arises how "pure" these measurements are since the question of third harmonic generation was never addressed.

A.2 Experimental Setup for Quantum Interference

As in any interferometric experiment it's crucial that the optical components have a good quality. Early experiments indicated that the mirrors and beam splitters were not flat enough for interferomentric experiments. To study the flatness of the optical components in the setup a simple Michelson interferometer was constructed. The oscillator pump laser (Coherent Verdi, $2 \times$ Nd:Yag) was expanded using a home made telescope so it completely filled the ½ inch pinhole used in the setup. The mode quality of this laser was good and no spatial filtering was needed. A $\lambda/50$ mirror was used as a reference together with a high quality beam splitter. The measurement revealed that the beam splitter mounts applied too much stress making the beam splitters twist. These beam splitters were replaced with ticker ones and placed in better mounts. The mirrors had a flatness of better than $\lambda/2$ over the aperture and the fringes showed a large curvature, indicating a weak spherical distortion.

Direct phase matched third harmonic (TH) generation in a nonlinear crystal is generally not possible due to the large dispersion in the refractive index. The traditional way of solving this problem employs frequency doubling, followed by sum frequency generation (SFG) and requires two different crystals (in our case, 1 mm BBO SHG type1 and 0.1 mm KDP, SFG type 2). Even if the group velocity mismatch in both crystals leads to low conversion efficiency, it was found that the signal was more than enough for the experiment. This method has one serious limitation. The second harmonic (SH) generation was very efficient and even after the SFG crystal there was a lot of SH present in the system. A high concentration solution of DTDCI (Lambdachrome, Lambda Physik) was prepared in a 1 mm cuvette and placed in the beam path. This solution was almost capable off cutting of the SH but it also introduced losses at the fundamental wavelength. The dispersion properties of the solution is not known but it is not unreasonable to assume that the third harmonic pulse would experience substantial broadening when transmitted trough this solution. Since we expect that both power and temporal overlap would be important it was decided to abandon this idea.

Estimating the optical density of the organic film used for third harmonic generation was not straight forward. The optical density of the film was very high and it could not be directly measured with the spectrometer due to saturation of the detector. The red tail of the absorption spectrum was not saturated and by measuring the (unsaturated) spectrum of the

chromophore in solution (dichloromethane) and rescaling the sample spectrum to the red tail it was possible to estimate the optical density. The optical density of the sample was estimated to be ~750. This is order of magnitude estimation since it is not clear that the spectra in gel and in solution are identical.

Finding the temporal overlap was not trivial. In our experiment we had the possibility of studying another interference pattern, namely interference between two three-photon transition amplitudes. This kind of interference is easier to observe since one can use a thicker sample (more signal) for a coarse determination of the time delay and then switch to a thinner sample. One does not need to align the beams perfectly since the signal will be drastically enhanced (10 times) when interfering (non-interferometric). The fringes are also easier to find since the angle between the beams can be larger and still give rise to visible fringes.

A.3 Techniques for Measurement of Pulse Duration

It's important to know the temporal shape of the pulses since the visibility of the interference pattern will depend on the temporal overlap of the fundamental- and the third harmonic-pulses. Experimental determination of the pulse durations are therefore of great interest for the quantum interference experiment.

Measuring the pulse shape of the fundamental is straight forward using second order autocorrelation (SHG) [36]. Pulses in the IR are easy to phase match in any nonlinear crystal. The task of measuring the duration of the third harmonic is a bit more complicated. Phase matching becomes more difficult for shorter wavelengths as the resulting second harmonic will be further in the UV region of the spectrum. It is in principle possible to generate second harmonic in BBO for a fundamental radiation of 415 nm, but it's difficult to achieve in practice. A more convenient way is to use sum frequency generation (SFG) between 415 nm (TH) and 1245 nm (F). It has two distinct advantages over SHG. First of all, the phase matching angle is close to the angle where our non-linear crystals are cut (for SHG in the NIR region). The other advantage is that the resulting radiation is around 311nm for 1245+415 nm which is easily detected using a standard photo multiplier.

The experimental setup from the quantum interference experiment was used for the measurement of the pulses. The crystal was placed at the position of the sample and the delay line was controlled by a stepper motor (Newport 850 G) and the signal from the detector was

monitored on a PC. Detection of the SHG was done with a photodiode (1621, New Focus) while a photo multiplier (Hamamatsu, HC120-05) was employed for the SFG measurement. Two different nonlinear crystals were available for this measurement, a 1mm BBO cut at θ=23° and a 0.1 mm KDP cut at θ=44°. Both crystals are negative uniaxial and since the polarization was the same (vertical) for both beams, type 1 phase matching was the natural choice. Phase matching angles, group velocity mismatch and broadening were calculated from the dispersion data of BBO and KDP [37] and are presented in table A.3.1. Note that when the crystal is rotated one needs to take into account the refractive index of the crystal to calculate the incident angle, for phase matching inside the sample. For the case of SFG, this becomes ambiguous (in collinear geometry) and we could not achieve perfect phase matching in our geometry.

Crystal	Thickness [mm]	Process	Phase matching angle θ [deg]	Crystal angle [deg]	Δu [fs mm^{-1}]
BBO	1	SHG	20.8	-3.6	0
BBO	1	SFG	33.3	17.2	336
KDP	0.1	SHG	26	28.3	0
KDP	0.1	SFG	49.3	-7.2	202

Table A.3.1. Phase matching angles and broadening (Δu) in BBO and KDP for SFG (ω+3ω) and SHG (ω+ω) of fundamental (1245 nm) and its third harmonic (415 nm)

The spectra of the two pulses were measured by sending light scattered from a piece of paper into a spectrometer (Triax 550, Jobain Yvon, 300 lines mm^{-1}). The spectrum of the fundamental and the third harmonic was detected with an IR detector (PDA 400, Thorlabs) and a PMT (HC120-05, Hamamatsu), respectively

Both in the case of auto- and cross correlation the measured signal is a convolution between two pulses. It is trivial, with the help of the transform rules for the Fourier transform, to show that the relationship between the measured and intrinsic pulsewidths is,

$$\Delta^2 = \delta_1^2 + \delta_2^2 \quad (5.4.1)$$

where δ_i is the FWHM of pulse i. We thus find that the measured signal for the auto correlation is $\sqrt{2}$ times broader than the actual pulse width. Equation 5.4.1 can be used to calculate the intrinsic pulse width for the cross correlation.

An often quoted property of ultra short pulses is the time-bandwidth product. The value of the time bandwidth product is an indication of the quality of the pulses in the sense that a transform-limited pulse will have the lowest possible value of the time bandwidth product. These values will be different for different pulse shapes and we consider only the Gaussian shape. Defining the FWHM of the frequency spectrum as Δv, one can show that the product of the pulse duration and frequency spread is

$$\Delta v \cdot \tau = 0.441$$

for a Gausian pulse without chirp. Any excess chirp will lead to a higher value of the time bandwidth product.

A.4 Measurement of Pulse Duration of Fundamental and Third Harmonic

Figure A.4.1a and b show the SHG- and the SFG-trace. The second order autocorrelation was interferometric since the beams are collinear. It was found that a step size of 2*100 nm was sufficient capture the features of the trace. Due to fluctuation in laser power a short integration time was used and the sum of five traces is displayed in figure A.4.1a. The trace does not follow the predicted curve with respect to peak to background value [36]. We also note that the cancellation for zero time delay is not complete due to not perfect alignment. The SHG trace was the same for both crystals but a large difference is evident in the SFG traces. In the SHG measurement both pulses travel with the same group velocity and the measured trace is independent of the crystal thickness. This is not the case for SFG. The trace becomes broadened due to large difference in group velocity between fundamental and third harmonic. Changing to the thinner KDP crystal revealed a narrower trace. There was still a substantial contribution from broadening in the crystal (20 fs) but a rough estimation of the duration of the third harmonic could be made. The width (FWHM, in KDP) of the traces was found to be 100 fs and 230 fs for the SHG and SFG, respectively.
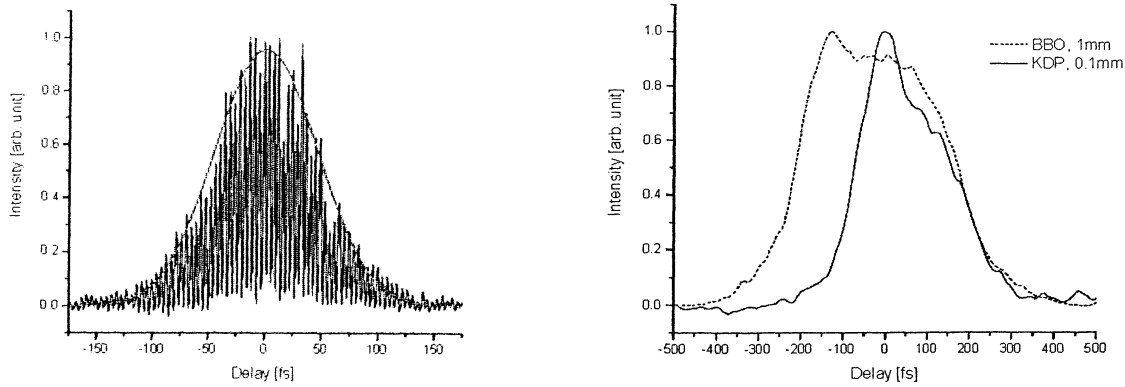
Figure A..4.1a and b. (left) Second order autocorrelation of fundamental. Red curve is a Gaussian fit. (right) Sum-frequency generation using fundamental and third harmonic. (Dotted) 1mm BBO, (solid) 0.1 mm KDP.

A Gaussian fit to the SHG trace worked reasonably well and a (Gaussian) de-convolution gave a pulse duration of 70 fs for the fundamental. This pulse could now in principle be used to de-convolve the SFG trace. We see that the SFG trace is asymmetric. From the available data were not able to tell if this asymmetry is due the fundamental or due to the third harmonic pulse since the SHG trace is always symmetric. Visual inspection of the SHG trace showed an interesting feature. The fringes turned from vertical to horizontal as the delay was changed. This could indicate some kind of asymmetry in the pulse. The asymmetry together with the fact that the broadening in the crystal can't be neglected (10%) makes this kind of de-convolution a bit arbitrary. An upper estimate of the pulse duration of the third harmonic can be made by subtracting the broadening and the width of the fundamental. This upper estimate gives duration of about 140 fs. Another way is to fit a Gaussian function to one of the sides of the trace. Fitting a Gaussian to the left side of figure A.5.1.b and then de-convolute this Gaussian with the fundamental gives a duration of approximately 110 fs. It must be noted here that it is not the actual duration of the third harmonic that is measured. Passing though the second beam splitter (see setup) affects the pulse in many ways. The interesting point in this case is the actual duration at the sample and not the "intrinsic" duration and it was decided not to modify the interferometer for such a measurement. A simple way to estimate the broadening due to the passage though the last beam splitter is to place a piece of glass after the interferometer. The SFG trace, with glass, is shown in figure A.4.2.
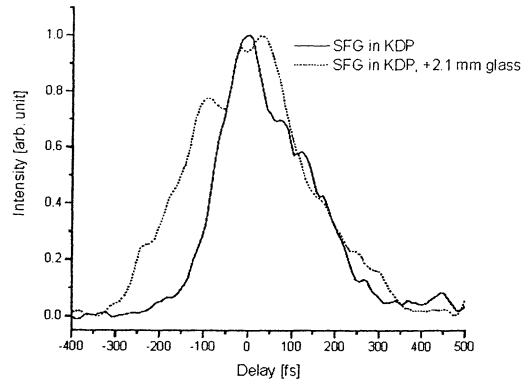
71

Figure A.4.2. Sum frequency generation in 0.1 mm KDP crystal. Dashed line is the trace obtained when 2.1 mm glass was placed after the interferometer. The solid line is the trace without glass.

The trace broadened significantly when the glass plate was inserted. Since the UV pulse is delayed by the glass the trace has been shifted so that the zero time delay is the same. The SFG trace broadened about 50 fs for a 2.1 mm transparent glass plate. The second beam splitter in the setup was 2.3 mm thick and it is on a BK7 substrate. Numerical estimation of the pulse broadening of the third harmonic gives ~40 fs for a spectral width of 15 nm. This is in good agreement with the experimental observations considering that the pulses are not transform limited and that self phase modulation is neglected. For the rest of this text it will be assumed that the pulse durations, at the sample, are 70 and 110 fs for the fundamental and third harmonic respectively.

The spectra of the fundamental and the third harmonic is shown in figure A.4.3 a and b
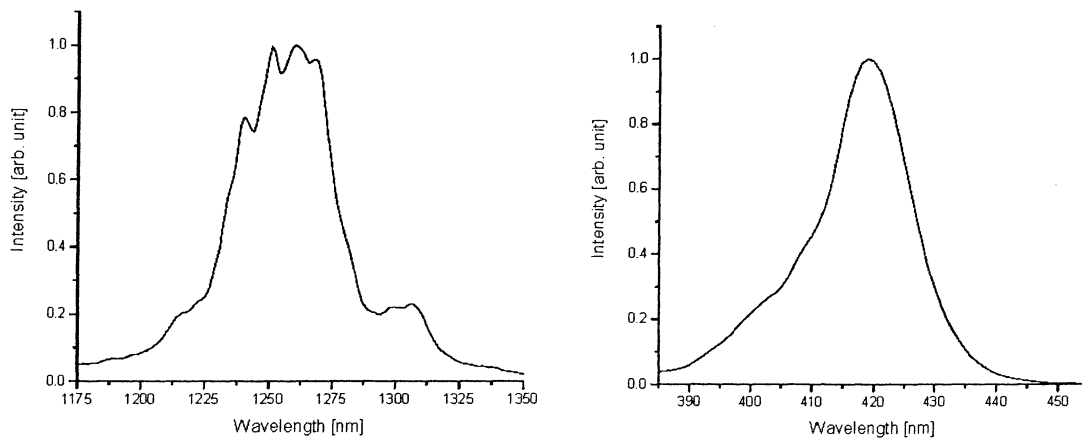
Figure A.4.3a and b. (left) Third harmonic spectrum. (right) Spectrum of the fundamental.

The spectra are rather broad with a FWHM of $0.99 \cdot 10^{13}$ Hz (fundamental) and $2.69 \cdot 10^{13}$ Hz (harmonic). It is interesting to note that the spectral width of the third harmonic is almost 3 times larger than the IR pulse. The fundamental spectrum shows a small modulation while the third harmonic is smoother. It is not clear why the harmonic has a broader tail on the blue side.

Since it is not possible to measure the autocorrelation of the third harmonic it is difficult to estimate the time-bandwidth product for this pulse. For the fundamental this is straight forward and we find that the time bandwidth product is ~0.7, roughly two times the theoretical limit for a Gaussian pulse shape. Both the time-bandwidth product and the pulse duration are in line with the specifications given by the manufacturer.
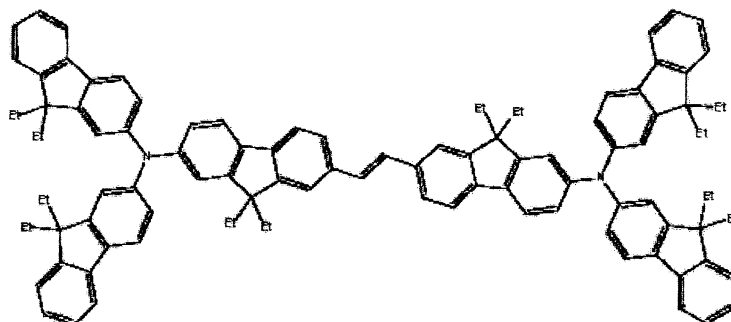
Appendix B

Chemical structure of the investigated compounds. G-0 hybrid and the molecule used for third harmonic generation are shown in section 5.2 and 5.1 respectively.
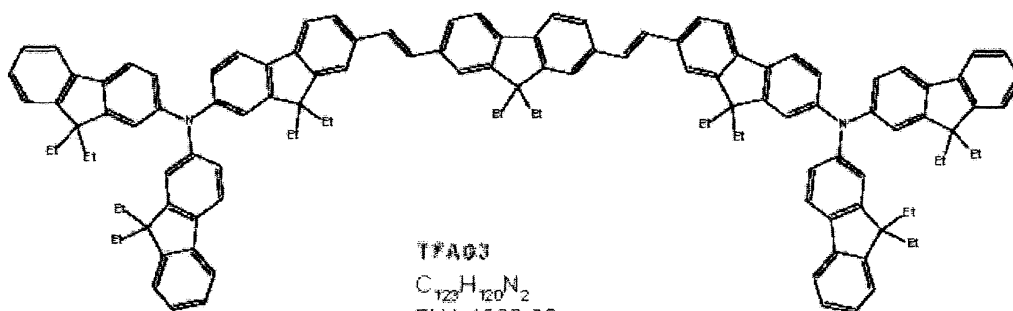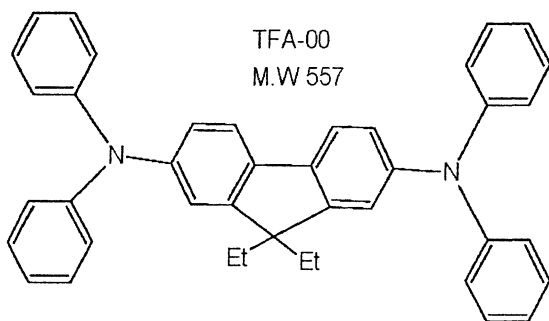
BDPAS
M.W 514

OM 67C
M.W 1096

OM 82C
M.W 2748

OM 87C 2
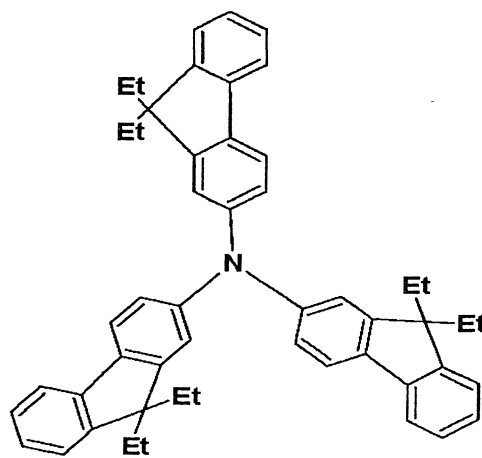**M.W 6053**
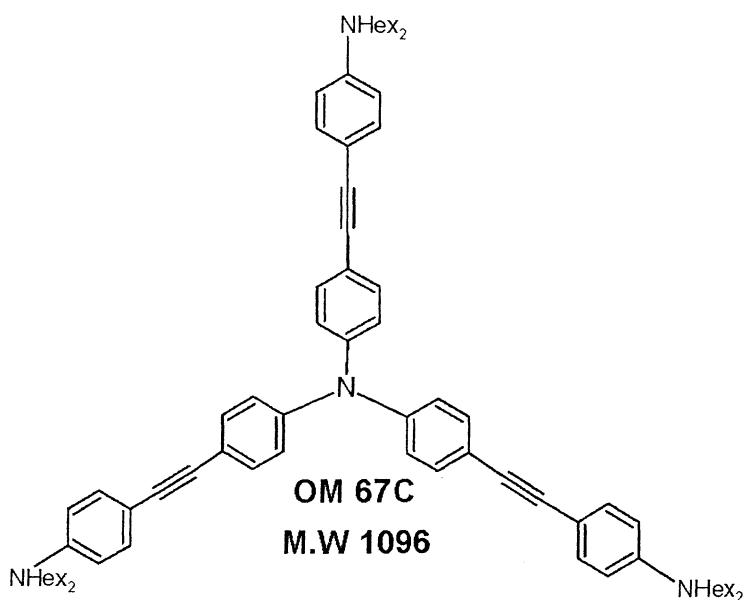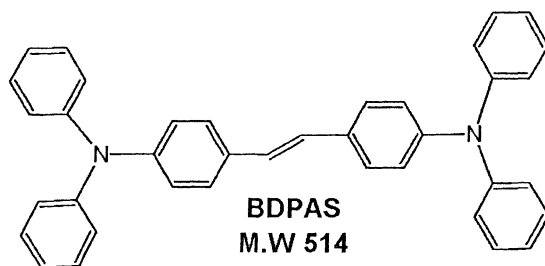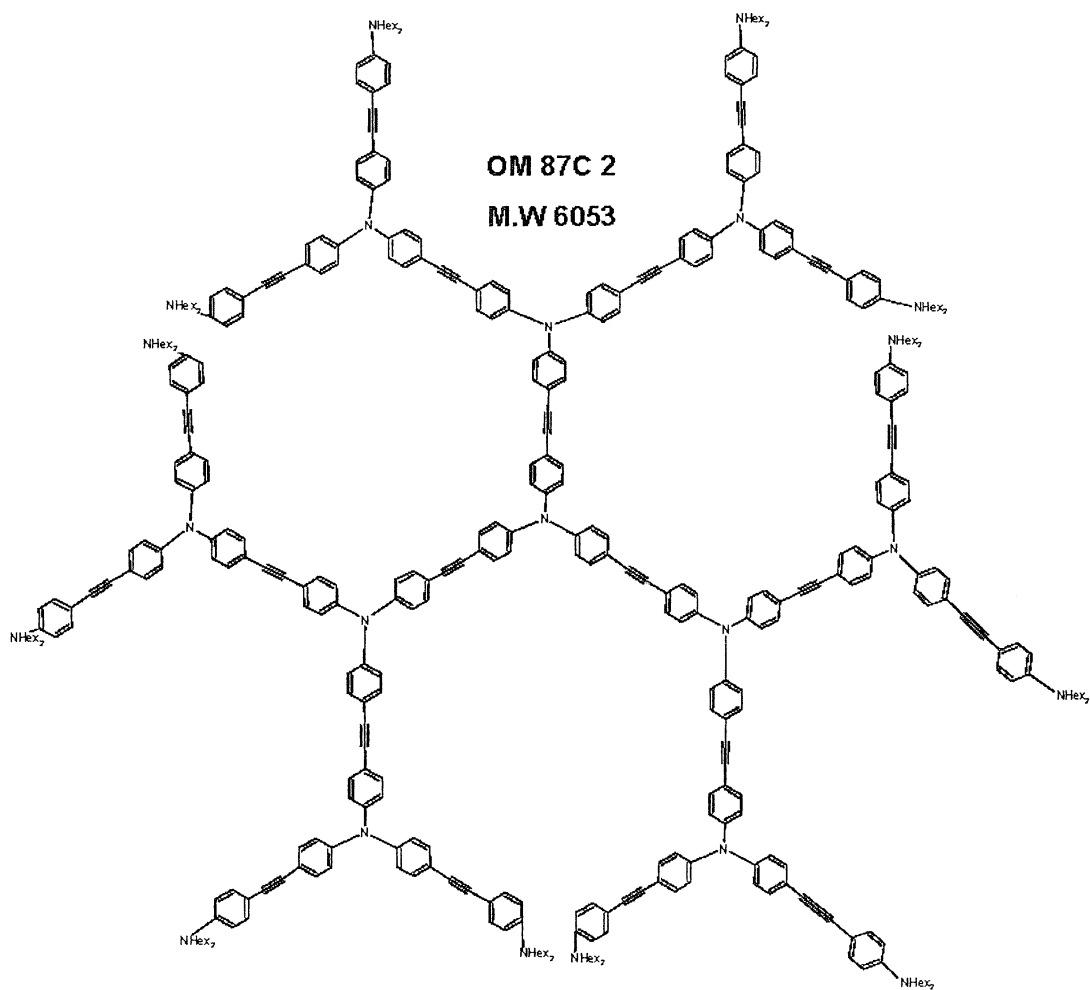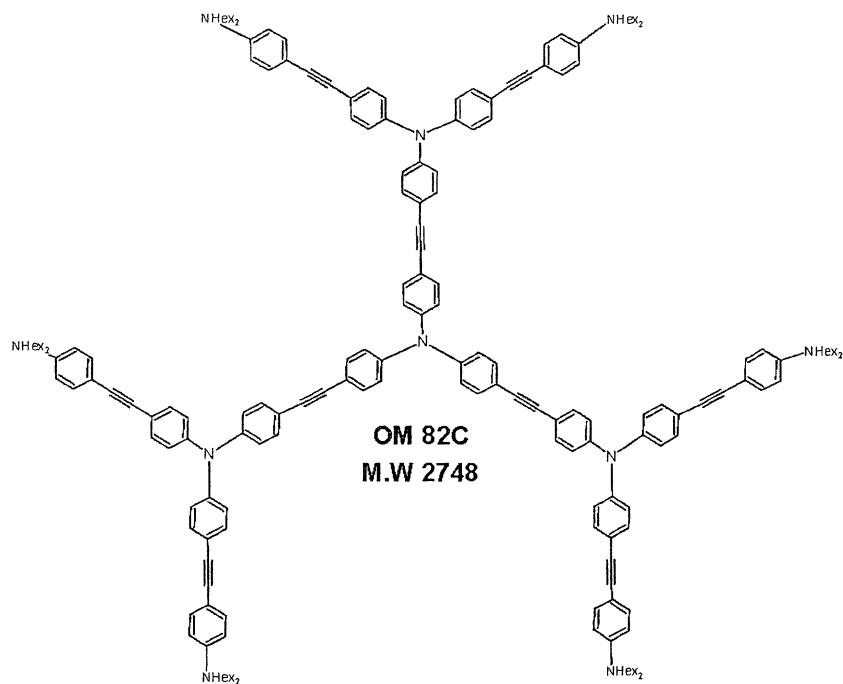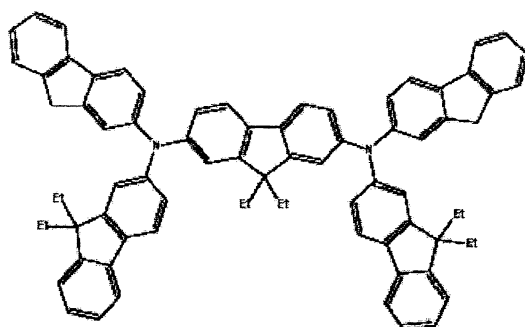
TFA01
$C_{77}H_{88}N_2$
FW=1021.38

TFA02
$C_{104}H_{102}N_2$
FW=1379.94

TFA03
$C_{123}H_{120}N_2$
FW=1626.28

TFA-00
M.W 557

3-Arm TFA
M.W 678

References

[1]   E. A. Manykin and A. M. Afanas'ev, Sovjet Physics, Jł
        E.A Manykin , "*Quantum interference and Coherent co*₁.₁₁ (60-67) 2001

[2]   X. Wang, R. Bersohn, K. Takahashi, M. Kawasaki and ł *of absorption in large   polyatomic molecules*", Journal of Chemical ph 996

[3]   R. Bersohn, "*Coherent control of photoexcitation proces*
        Journal of Molecular structure, 480-481 (231-235), 1999

[4]   L. Zhu, V.D. Kleinman, X. Li, R.J Gordon, Journal of ch

[5]   M. Shapiro and P. Brumer, "*Coherent control of molecuł*
        Reports on progress in physics, 66 (859-942), 2003

[5]   R. J. Gordon, L. Zhu and T. Siedeman, "*Using the phase* ₄ical tool"
        Journal of chemical physics A, 105 (4387-4393), 2001

[6]   M. Dantus and V. V. Lazovoy, "*Experimental coherent la*ʰemical processes"
        Chemical review, 104 (1813-1859), 2004

[8]   J.M. Fraser and H.M van Driel,, "*Quantum Interference co*ʰdensity in GaAs",
        Physical review B, 68 (085208) ,2003

[9]   R.W. Boyd, "*Nonlinear optics* ", 2:nd edition, Academic Prc

[10]   B.H. Bradsden and C.J. Joachain, "*Physics of atoms and mo*ₗon, Prentice Hall, 2003, Malaysia

[11]   A. Karotki, "Simultaneous Two-Photon Absorption of Tetraķ: From Femtosecond
        Coherence Experiments to Photodynamic Therapy", DoctoralState University 2003.

[12]   L.Zhu, X. Yang, Y. Yi, P. Xuan, Z. Shuai, D. Chen, E. Zojer,ı. Beljonne, "*Three-photon   absorption in anthracene-rphyrin-anthracene triads:*ʰical study",
        Journal of chemical physics, 121 (11060-11067), 2004

[13]   A. Brown and W. J Meath, "*Role of permanent dipoles and or*ₐging in the phase control of two-   color, simultaneous one- and three- photon molecular*
        Physical review A, 53 (2571-2586), 1996

[14]   W. J. Meath and E. A. Power, "*On the importance of permanen*multiphoton absorption using perturbation theory*", Journal of physics B: Atomic and mics, 17 (763-781), 1984

[15]   A. Apostoluk, D. Chapron, G. Gadret, B. Sahraoui and J. M. Nuphase-matched gratings printed   by all optical poling in polymer films* ", Optics letters, 2ı), 2002

[16]   A. Apostoluk and J. M. Nunzi,, "*Photoinduction of surface relie*jring all-optical poling of polymer films* ", Optics letters, 29 (98-100), 2004

[17]   S. Bidault, S. Brasselet and J. Zyss, "*Coherent control of the opti*ar and luminescence anisotropies in molecular thin films by multiphoton excitations* " ,₂rs 29 (1242-1244), 2004

[18]   D. Petrosyan and P. Lambropoulos, "*Phase control of resonantly* ohotoionization in an optically dense   medium* ", Physical review A, 63 (043417), 2001

[19]   A. Bree, A. Leydermann and C. Taliani, "*Competition between se*aonic generation and one- and two-photon absorption in the anthracene/9,10-dihydroanthraci crystal",

Journal of Applied physics, 62 (4662-4667),1987

[20]   H.S Nalawa and S. Miyata, "Nonlinear optics of Organic molecules and Polymers",

chapter 11. CRC Press, Boca Ranton, USA 1997

and

M. G. Kuzyk and C. W. Dirk, "Characterization Techniques and Tabulations for Organic nonlinear optical materials", Marcel Decker, New York, USA, 1998

[21]   M. Drobizhev, A. Karotki, M. Kruk, Y. Dzenis, A. Rebane, Z. Sou and C. W. Spangler, *"Uncovering coherent domain structure in a series of π-conjugated Dendrimers by simultaneous three-photon absorption"*,

Journal of physical chemistry B, 108 (4221-4226), 2004

[22]   O. Svelto, *"Principles of lasers"*, 4:th edition, Plenum Press, 1998, USA, Manuals for Coherent MIRA (oscillator), CPA-1000 Clark MXR (amplifier) and Quantronix TOPAS (OPA).

[23]   J. Swiatkiewicz, P. N. Prasad and B. A. Reinhardt, *"Probing two-photon excitation dynamics using ultrafast laser pulses"*, Optics communication, 157 (135-138), 1998

[24]   M. Drobizhev, A. Rebane, Z. Sou and C. W. Spangler,

"One-, two- and three-photon spectroscopy of π-conjugated Dendrimers: Cooperative enhancemenat and Coherent domains", Submitted to Journal of Luminescence, 2004

[25]   C. Zhan, D. Lei, D. Zhang, Y. Li, D. Wang, T. Wang, Z. Lu, L.Zhao, Y. Nie and D. Zhu, *"Three-photon absorption from six stilbazolium derivatives: application for optical limiting"*,

Chemical physics letters, 353 (138-142) 2002

[26]   J. E. Ehrlich, X. L.Wu, I-Y. S. Lee, Z-Y. Hu, H. Rockel, S. R. Marder and J. W. Perry, *"Two-photon absorption and broadband optical limiting with bis-donor stilbebenes"*,

Optics letters, 22 (1843-1845), 1997

[27]   H. Hacken and H. C. Wolf, *"Molecular physics and elements of quantum chemistry: Introduction to experiments and theory"*, Springer Verlag, 1995, Germany

[28]   N. S. Bayliss, "A metallic model for the spectra of conjgated polyenes"

Journal of chemical physics, 16 (287-291), 1948

[29]   S. J. K Pond et al, "Excited state dynamics of BDPAS"

Journal of physical chemistry A, 106, (11470-11480), 2002

[30]   S. Svanberg, *"Atomic and molecular spectroscopy"*, 3:rd edtition, Springer Verlag, 2001, Germany

[31]   F.E. Hernandez, K. D. Belfield, I. Cohanoschi, *"Three-photon absorption enhancement in a symmetrical charge transfer fluorene derivative"*,

Chemical Physics Letters, 391 (22-26), 2004

[32]   S. Maiti, W. Zipfel, J. B. Shear, R. M. Williams and W.W. Webb, *"Measuring Seratonin Distribution in live cells with three-photon excitation"*, Science, 275 (530-532), 1997

[33]   J.R. Cable and A.C. Albrecht, "A *condenced phase study of the Benzene B_{2u}-A_{1g} three-photon transition"*,

Journal of chemical physics, 85 (3155-3164), 1986

[34]   N. G. Sultanova, I. D Nikolov and C. D. Ivanov, *"Measuring the refractometric characteristics of optical plastics"*, Optical and Quantum electronics, 35 (21-34), 2003

[35]   F.L: Pedrotti and L.S. Pedrotti, *"Introduction to optics"*, 2:nd edition, Prentice Hall, 1996, USA

[36]   J. C Diels, "Ultrashort laser pulse phenomena: fundamentals, techniques and applications on a femtosecond time scale", Academic Press, USA, 1996

[37]   P. Langlois and E. P. Iippen, *"Measurement of pulse asymmetry by three-photon absorption aoutocorrelation in a GaAs photodiode"*, Optics Letters, 24 (1868-1870), 1999

[38]   Dispersion data, www.cvilaser.com (BK7), www.unitedcrystals.com (BBO and KDP)

[39]   P.M. Dirac, *"The principles of quantum mechanics"*, 4:th edition, Oxford University Press, 1958, UK

[40]   D-I. Lee and C. Roychoudhuri, *"Measuring properties of superimposed light beams carrying different frequencies"*, Optics express, 11 (944-951), 2003

[41]   J. J. Wynne, *"Nonlinear optical balance"*, Multiphoton processes, Proc. Of 4 th International Conference on multiphoton processes, ed. S.J Smith and P.L Knight, Cambridge University. Press, Cambridge, UK, 1998

[42]   T. Nakajima, *"Propagation of phase controlled lasers in a two-level medium"*, Physical review A 64 (043406), 2001

[43]   X. Song, S. Gong, S. Jin and Z. Xu, *"Two-color interference effects for ultrashort laser pulses propagating in a two-level medium"* , Physics letters A, 319 (150-156) ,2003

[44]   C. Chen and D. S. Elliot, *"Propagation effects in two color coherent control processes"*, Physical review A, 53 (272-279), 1996